map3k1 is required for spatial restriction of progenitor differentiation in planarians

Bryanna Isela-Inez Canales[1,2], Hunter O. King[1,3], and Peter W. Reddien[1,2,4,*]

[1]Whitehead Institute for Biomedical Research, Cambridge, MA 02142, USA.

[2]Department of Biology, Massachusetts Institute of Technology, Cambridge, MA 02139, USA.

[3]Department of Brain and Cognitive Sciences, Massachusetts Institute of Technology, Cambridge, MA 02139, USA

[4]Howard Hughes Medical Institute, Massachusetts Institute of Technology, Cambridge, MA 02139, USA.

*Corresponding author. Email: reddien@wi.mit.edu

Planarian regeneration and tissue turnover involve fate specification in pluripotent stem cells called neoblasts. Neoblasts select fates through the expression of fate-specific transcription factors (FSTFs), generating specialized neoblasts. Specialized neoblasts are spatially intermingled and can be dispersed broadly, frequently being far from their target tissue. The post-mitotic progeny of neoblasts, serving as progenitors, migrate and differentiate into mature cell types. Pattern formation is thus strongly influenced by the migratory assortment and differentiation of fate-specified progenitors in precise locations, which we refer to as progenitor targeting. This central step of pattern maintenance and formation, however, is poorly understood. Here, we describe a requirement for the conserved *map3k1* gene in targeting, restricting post-mitotic progenitor differentiation to precise locations. RNAi of *map3k1* causes ectopic differentiation of eye progenitors along their migratory path, resulting in dispersed ectopic eyes and eye cells. Other neural tissues similarly display ectopic posterior differentiation and pharynx cells emerge dispersed laterally and anteriorly in *map3k1* RNAi animals. Ectopic differentiated cells are also found within the incorrect organs after *map3k1* RNAi, and ultimately teratomas form. These findings implicate *map3k1* signaling in controlling the positional regulation of progenitor behavior – restricting progenitor differentiation to targeted locations in response to external cues in the local tissue environment.

Introduction

Planarians are capable of regenerating any missing body part through the action of pluripotent stem cells called neoblasts (Reddien, 2018). Neoblasts also maintain all cell types of the adult body through a process of constitutive cell turnover. Because planarians have >125 different adult cell types, these stem cells must be capable of choosing among a large array of possible cell fates (Fincher et al., 2018; Plass et al., 2018; Zeng et al., 2018; King et al., 2024). Fate specification can occur in neoblasts through the activation of transcription factors called fate-specific transcription factors (FSTFs), producing specialized neoblasts (Reddien, 2022). Specialized neoblasts divide and can produce daughter cells that act as migratory precursors (post-mitotic progenitors) for differentiated cell types (Eisenhoffer et al., 2008; van Wolfswinkel et al., 2014; Reddien, 2022; King et al., 2024).

Fate choice in neoblasts can be regulated by position. For instance, eye-specialized neoblasts are formed in roughly the anterior third of the animal (Lapan and Reddien, 2011, 2012). However, this spatial regulation of stem cell fate specification is coarse, when compared to the precise positioning of cell differentiation to form functional, complex tissue architecture (Lapan and Reddien, 2011, 2012; Adler et al., 2014; Scimone et al., 2014a; van Wolfswinkel et al., 2014; Park et al., 2023). Because specialized neoblasts are produced in broad regions, they are often found far from their target tissue. Indeed, specialized neoblasts can frequently be found closer to other differentiated cell types than to the differentiated tissue they are fated to mature into (Park et al., 2023). Furthermore, neoblasts are specified in a highly spatially intermingled manner, in heterogenous neoblast neighborhoods (Park et al., 2023). For instance, a muscle-specialized neoblast could have a neural, intestinal, epidermal, eye, or other specialized neoblast as its nearest neoblast neighbor (Park et al., 2023). These observations suggest that the regulation of differentiation programs for post-mitotic migratory progenitors is a crucial aspect to patterning and maintaining the various tissues in the animal. Neoblasts themselves are not highly migratory, however (Saló and Baguñà, 1985; Guedelhoefer and Sánchez Alvarado, 2012; Abnave et al., 2017). By contrast, the post-mitotic descendant cells of neoblasts can remain immature for a number of days – serving as progenitors – and can be migratory (Eisenhoffer et al., 2008; Wenemoser and Reddien, 2010; Guedelhoefer and Sánchez Alvarado, 2012; van Wolfswinkel et al., 2014; Abnave et al., 2017; Park et al., 2023). These findings generate a model for pattern maintenance during tissue turnover and formation in planarian regeneration in which specialized neoblasts generate post-mitotic progenitors that assort and target precise locations for differentiation through migration (Park et al., 2023).

From a messy state of planarian progenitor formation, order must arise. Terminal differentiation of post-mitotic progenitors must be regulated to occur at precise positions to prevent disordered differentiation along migratory trails. Defects in this process could lead to errors in tissue pattern, such as supernumerary organs, ectopic differentiation of single cells, incorrect incorporation of a particular cell type into the wrong tissue, and teratoma formation. Therefore, understanding how migratory progenitors know when and where to terminally differentiate into a mature stationary cell is a central problem for understanding how systems of migratory progenitors generate and maintain pattern. Little is known about the molecular regulation of differentiation, restricting it to occur in precise locations. Given that progenitor migratory targeting and differentiation are the predominant processes involved in planarian adult tissue patterning, identification of the molecular processes regulating these behaviors is central for understanding adult regeneration and pattern maintenance. Planarians present the opportunity to uncover general mechanisms underlying migratory progenitor targeting and differentiation regulation, which could apply to a myriad of developmental and regenerative contexts across the animal kingdom.

Results

map3k1 *RNAi results in the ectopic posterior differentiation of eye cells along the AP axis.*

We sought to understand how the differentiation of fate-specified progenitors is spatially regulated to control planarian patterning through RNAi studies. The RNAi of a single gene (*map3k1,* dd_5198) encoding a MAP3K1-like signaling protein resulted in a striking phenotype of ectopic eye formation that was distinct in nature from previously described planarian patterning phenotypes, and was suggestive of having a candidate role in progenitor targeting (Figure 1A). We therefore selected this gene for detailed investigation given the robust and unique nature of its patterning phenotype. Planarian *map3k1* encodes a member of the MAP3K1 subclass of MAP3K signaling proteins. MAP3K1 proteins, including the planarian ortholog, possess a unique domain architecture among MAP3Ks. Aside from its characteristic kinase domain, MAP3K1 has other unique domains: a PHD-like RING finger, a SWIM-type RING finger, and a TOG-like domain. These domains have been implicated in non-canonical MAP kinase signaling cascades that enable MAP3K1 to act as a ubiquitin ligase, a scaffold protein, and to signal through MAP kinase proteins (Figure 1- figure supplement 1).

The bilaterally symmetric anterior location of planarian eyes represents the normal targeting location of eye progenitors (Lapan and Reddien, 2011, 2012). RNAi of *map3k1*

114 resulted in the gradual emergence of ectopic eyes posterior to the normal eye location (Figure
115 1A,B). Ectopic eyes displayed some variance in their posterior and medial-lateral (ML) positions
116 in the pre-pharyngeal animal region (Figure 1A,B). Fluorescent in situ hybridization (FISH)
117 experiments showed that both optic cup and photoreceptor cells were present ectopically
118 (Figure 1A,B). Ectopic optic cup and photoreceptor cells were observed both as clusters of cells
119 that nucleated and grew into additional eyes, as well as individual, isolated eye cells (Figure
120 1A,B; Figure 1- figure supplement 1B). Isolated, individual photoreceptor neuron or optic cup
121 cell differentiation is rarely observed in the wild-type state. Surprisingly, although ectopic eye
122 cells appeared most frequently in the normal zone of eye progenitor specification, they also
123 appeared along the entire AP axis, including in the posterior half of the tail – far from the normal
124 eye-progenitor specification zone (Figure 1C, Figure 1- figure supplement 1B). Most animals
125 had at least one ectopic eye cell in the tail after 26 days of *map3k1* RNAi. The *map3k1* RNAi
126 phenotype did not appear to result from a anterior-to-posterior progression of eye formation,
127 because isolated eye cells were observed in RNAi animal tails even at early RNAi timepoints
128 when no, or very few other ectopic differentiated eye cells appeared between the head and tail
129 (Figure 1C, F, Figure 1- figure supplement 1B). The very posterior ectopic eye cells that
130 appeared in *map3k1* RNAi animals were more sparse than those in the head, and more likely to
131 appear as singletons rather than aggregates (Figure 1C, Figure 1- figure supplement 1B).
132 The location where dispersed eye progenitors migrate towards and undergo terminal
133 differentiation is referred to as the target zone (TZ) (Atabay et al., 2018). A variety of genes can
134 be inhibited to result in eye formation in ectopic positions along the anterior-posterior (AP) axis:
135 for instance, posteriorly for RNAi of *nou darake (ndk)* (Cebria et al., 2002) or *wntA* (Kobayashi et
136 al., 2007), and anteriorly for RNAi of *notum* (Hill and Petersen, 2015) and *nr4A* (Li et al., 2019).
137 Furthermore, *wnt5* RNAi causes ectopic lateral eye formation and *slit* RNAi cause medial eye
138 formation (Oderberg et al., 2017; Atabay et al., 2018). However, in all of these cases ectopic
139 eyes appear along particular AP or ML trajectories (Figure 1D, summary cartoon), consistent
140 with alteration of the eye progenitor TZ along a single (AP or ML) axis, but still with
141 differentiation constrained to occur in a particular position on the orthogonal axis. By contrast,
142 *map3k1* RNAi ectopic eyes were more diffuse, often being ectopic in both AP and ML position.
143 This distinct patterning phenotype raised the possibility that *map3k1* was required for a
144 patterning process not previously perturbed by inhibition of prior patterning genes.
145 Patterning in planarians prominently involves constitutive and regional expression of
146 genes constituting positional information referred to as position control genes (PCGs) (Reddien,
147 2018). PCGs are predominantly expressed in planarian muscle (Witchley et al., 2013). *slit, wnt5,*

148 *ndk, nr4A,* and *notum* are regulated in their spatial expression and are components of this PCG
149 patterning system. Therefore, these genes likely influence progenitor-extrinsic cues that guide
150 progenitor targeting. By contrast, *map3k1* is not expressed overtly in a spatially restricted
151 manner, instead being expressed broadly across tissues (Figure 1- figure supplement 1C).
152 The appearance of eye cells in the tail of *map3k1* RNAi animals suggests that some eye
153 progenitor specification is likely occurring in the tails of these animals. Eye specialized
154 neoblasts can be recognized by the co-expression of the eye-specific FSTF *ovo* (Lapan and
155 Reddien, 2012) and the neoblast marker *smedwi-1* (Reddien et al., 2005). Indeed, *ovo+;*
156 *smedwi-1+* neoblasts were observed at low frequency in the midbody and tail of *map3k1* RNAi
157 animals (Figure 1E; Figure 1- figure supplement 1D, E). The frequency of these observed rare
158 *ovo+* neoblasts was not substantially different from a low frequency observed in control animals,
159 raising the possibility that low frequency sporadic eye neoblast specification events in the body
160 can lead to ectopic differentiation when *map3k1* is inhibited.
161
162 **map3k1 *prevents the posteriorization of some but not all anterior cell types***
163 To assess whether the ectopic differentiation of progenitors that occurred in *map3k1* RNAi
164 animals was specific to the eye, we visualized other features of differentiated tissue patterns.
165 For example, lateral branches are normally associated specifically with the planarian brain
166 (Hyman, 1951). However, after *map3k1* RNAi, ectopic brain branches emerged from the two
167 ventral nerve cords – most commonly observed in the anterior and mid-body, extending to the
168 far posterior of the animal over long-term (>6 weeks) RNAi in uninjured animals (Figure 2A,
169 Figure 2- figure supplement 1A). Ectopic eyes sent axons that traveled along branches and
170 main nerve cord tracts (Figure 2A, Figure 2- figure supplement 1A). Ectopic brain branches that
171 emerged from ventral nerve cords contained *GluR*$^{+}$ neurons, confirming that they are at least
172 partly comprised of normally brain-branch-restricted neurons (Figure 2B). *GluR*$^{+}$ neurons are
173 similarly found in ectopic brain branches observed after RNAi of *ndk* (Cebria et al., 2002).
174 Another anterior neural population, marked with an RNA probe to dd_17258, also
175 displayed ectopic differentiation across the AP axis of *map3k1* RNAi animals – including through
176 to the tip of the tail (Figure 2C, Figure 2- figure supplement 1B,C). By contrast, the AP location
177 of *cintillo*$^{+}$ neurons, which display posteriorization in *ndk* RNAi animals (Scimone et al., 2016),
178 remained unaffected in *map3k1* RNAi animals (Figure 2C). Another anterior-restricted neural
179 population (*glutamic acid decarboxylase, gad+*) also failed to show posteriorization following
180 *map3k1* RNAi (Figure 2-figure supplement 1D). These findings suggest that *map3k1* is required
181 for the normal AP restriction of a subset of neural cell types during tissue turnover. The cell

182 types that displayed posteriorization following *map3k1* RNAi also maintained their general tissue
183 structure in their normal locations, rather than being lost anteriorly and replaced with a more
184 posterior domain.
185 To determine if tissue posteriorization occurred in non-neuronal cell types, we assayed
186 particular gland cell populations that predominantly reside in the head, with a small fraction
187 extending down to the pharynx and rarely to the tail. *map3k1* RNAi animals showed
188 posteriorization of gland cell distributions for the primarily anterior dd_7131+ and dd_8476+
189 populations (Figure 2D-F). As was the case with the neurons, not all gland cell types were
190 affected by *map3k1* RNAi. dd_9223+ cells, which are normally restricted to the anterior, did not
191 change in distribution (Figure 2D). These data indicate that *map3k1* broadly affects the spatial
192 distribution of differentiated cell types for multiple tissues during tissue maintenance through
193 turnover, but that its role in regulating differentiation is restricted to a subset of progenitor
194 populations.
195
196 **map3k1 *inhibition causes ectopic anterior differentiation of pharynx progenitors***
197 Another regional tissue that is maintained through turnover from regional progenitors is the
198 planarian pharynx. *FoxA* is expressed in neoblasts surrounding the centrally located pharynx,
199 specifying progenitors for this organ (Adler et al., 2014; Scimone et al., 2014a). These
200 progenitors must enter the pharynx through a connection to the body at the anterior end of the
201 organ. After *map3k1* RNAi, *vitrin*$^{+}$ pharynx cells appeared at the anterior domain of the predicted
202 *FoxA*+ zone, through which pharynx progenitors are migrating, as well more anterior to the
203 normal *FoxA*+ zone (Figure 3A). *vitrin*$^{+}$ cells clustered together to form small structures
204 containing pharyngeal cells between the original pharynx and the brain (Figure 3A). Most
205 animals developed one main ectopic pharynx cell cluster anterior to the original pharynx,
206 whereas others developed multiple anterior structures that could also exist lateral to the midline
207 (Figure 3A). This variable placement of ectopic pharyngeal cells on the ML axis is reminiscent of
208 the patterning defect observed with eyes described above. Interestingly, many progenitors in the
209 *FoxA* zone appear to differentiate as singletons – single pharynx cells, a phenotype not
210 previously observed with other patterning phenotypes, and also bearing similarity to the ectopic
211 eye cell defect.
212 The planarian mouth is an epidermal opening associated with the posterior end of the
213 pharynx. Ectopic anterior mouth cells marked by RNA transcripts for the gene *NB.22.1e* were
214 also observed following *map3k1* RNAi. Ectopic mouth cells appeared as an anterior streak of
215 cells with *NB.22.1e* transcripts, originating from the original mouth. In addition, ectopic sparse,

216 scattered mouth cells were also present, sometimes lateral to the midline (Figure 3B). Rarely
217 (n=2/12 animals), an ectopic focus of *NB.22.1e*+ mouth cells was observed in the tail, posterior
218 to the pharynx (Figure 3B). We also examined the pattern of cells expressing *mhc1*, which
219 marks pharyngeal muscle. Similar to the case of *vitrin*+ cells, scattered ectopic foci of
220 pharyngeal muscle cells were observed in the anterior half of the animal (Figure 3C).
221 Because differentiated pharynx cells were observed outside of the normal progenitor
222 specification zone, we considered the possibility that pharynx progenitor specification itself
223 occurred in ectopic locations following *map3k1* RNAi. dd_554 transcripts mark a post-mitotic
224 pharynx progenitor population (Zhu et al., 2015). Ectopic dd_554 cells were observed anterior to
225 the pharynx in *map3k1* RNAi animals, including in foci (Figure 3D). *FoxA*$^{+}$*; smedwi-1*$^{+}$ cells
226 include prominently pharynx progenitors. A small frequency of animals exhibited *FoxA*$^{+}$*;*
227 *smedwi-1*$^{+}$ cells between the lobes of the cephalic ganglia of long term *map3k1* RNAi animals.
228 This location is anterior to the normal progenitor specification zone for the pharynx (Figure 3E),
229 which is typically centrally restricted on the AP axis (Adler et al., 2014; Scimone et al., 2014a).
230 These findings are consistent with the interpretation that these *FoxA*$^{+}$*; smedwi-1*$^{+}$ cells possibly
231 include pharynx progenitors and that stem cell fate specification may occur outside of the
232 normally spatially restricted domains in *map3K1* RNAi animals, at least in the case of the
233 pharynx.
234 Complete posterior duplication of the pharynx has previously been observed with *ptk7,*
235 *ndl-3*, and *wntP-2* RNAi (Scimone et al., 2016; Hill and Petersen, 2018), anterior duplication has
236 been observed after *roboA* RNAi (Cebria and Newmark, 2007), and lateral duplication has been
237 observed after *wnt5* RNAi (Gurley et al., 2010). The *map3k1* RNAi phenotype differs from these
238 other patterning phenotypes, in that it involves greater disorganization, small clusters of
239 pharyngeal cells, and even single pharyngeal cells. This scenario bears similarity to the
240 phenotype for the eye: disorganized ectopic tissue differentiation including in small clusters and
241 single cells. These scenarios suggest defects in the regulation of progenitor targeting for
242 differentiation in precise locations.
243
244 ***The targeting and maintenance of tissues after* map3k1 *RNAi***
245 Post-mitotic progenitors normally migrate to their target zone (TZ) and differentiate at this
246 location. Prior work indicates that in addition to the TZ, the target tissue itself can incorporate its
247 fate-specified progenitors and promote progenitor differentiation, even in ectopic locations
248 (outside of the TZ) (Atabay et al., 2018; Hill and Petersen, 2018). For instance, surgical
249 manipulations (including transplantation) that lead to ectopic eyes outside of the TZ in wild-type

250 animals result in stable maintenance of those ectopic eyes through progenitor incorporation and
251 differentiation as part of turnover (Atabay et al., 2018). This is enabled by the fact that
252 progenitors in wild-type animals are specified in broad regions, giving ectopic differentiated
253 tissues access to a constant supply of progenitors (Lapan and Reddien, 2011, 2012). Thus, at
254 least two components appear to be capable of promoting progenitor differentiation: the TZ and
255 the target tissue. The pharynx shows similar properties to the case of the eye – with an ectopic
256 pharynx being maintained through progenitor incorporation and differentiation (Hill and
257 Petersen, 2018). A surgically transplanted ectopic organ (outside of its TZ), however, will not
258 regenerate upon its removal. Because the original TZ location of the tissue is unchanged,
259 progenitors will target the correct location after resection of an ectopic organ (Atabay et al.,
260 2018; Hill and Petersen, 2018).
261 Given the above reasoning, ectopic eyes in *map3k1* RNAi animals could in principle be
262 explained by TZ movement or expansion, if *map3k1* primarily acted to control TZ locations. To
263 assess whether TZ alteration, or some other explanation for the *map3k1* RNAi phenotype is
264 more likely, we resected all visible eyes in *map3k1* RNAi animals to determine the location of
265 new progenitor differentiation in the absence of a target tissue. These eye-resected *map3k1*
266 RNAi animals grew back eyes at a comparable rate to control animals, and in the expected wild-
267 type (normal TZ) location (Figure 4A). Notably, however, *map3k1* RNAi animals did not
268 regenerate all other ectopic eyes that were removed. This indicates that the TZ location is
269 maintained after *map3k1* RNAi, and that at least some progenitors are capable of migrating and
270 differentiating at the normal TZ location in the absence of an eye. These data are consistent
271 with a model in which *map3k1* does not primarily control the positional information read by
272 progenitors, but instead affects the ability of progenitors to differentiate at proper locations in
273 response to a normal positional information system – a possibility explored further below.
274 To determine if the pharynx target zone is also maintained in its normal, wild-type
275 location in *map3k1* RNAi animals, we removed the entire pharynx from its normal location
276 during progression of the *map3k1* RNAi phenotype (Figure 4B, Figure 4- figure supplement 1A).
277 By 10 days after pharynx resection, animals regenerated a pharynx in the original pharynx
278 position, as well as displayed an additional anterior pharynx-like structure (Figure 4B, Figure 4-
279 figure supplement 1B). Thus, the case for the pharynx is more complex than for the eye.
280 Regardless, these findings for the pharynx suggest that at least the normal central TZ remains
281 and is not simply shifted anteriorly.
282
283 ***The location of* de novo *organ regeneration after* map3k1 *RNAi***

284 To determine the location of progenitor targeting and de novo organ formation during
285 regeneration, we amputated *map3k1* RNAi animals into head, trunk, and tail fragments and
286 analyzed them after 10 days of regeneration. All fragments regenerated any organs that they
287 did not already contain at the time of amputation (Figure 4C, D). Two eyes formed in
288 approximately normal locations in *map3k1* RNAi head blastemas, rather than being posteriorly
289 shifted or appearing in multiple locations initially. This suggests, similarly to the results from the
290 eye resection experiments described above, that the TZ is regenerated in roughly the wild-type
291 location in *map3k1* RNAi animals.
292 Prior work in the planarian species *D. japonica* showed that *map3k1* RNAi results in tail
293 fragments regenerating pharynges in an anterior-shifted location (Hosoda et al., 2018).
294 Consistent with this previously reported effect, pharynges regenerated more anteriorly in
295 *map3k1* RNAi *S. mediterranea* tail fragments, just posterior to the regenerating brain (Figure
296 4C-E). Notably, trunks also regenerated secondary pharynx-like aggregates very close to the
297 brain that were underdeveloped, and appeared to interfere with structures around them (Figure
298 4D, E). Head fragments regenerated multiple pharyngeal structures (Figure 4- figure
299 supplement 1C). Therefore, the situation for the pharynx in regeneration is more complex than
300 that of the eye, similar to the findings for organ resections described above.
301
302 ***PCGs and pole organization are largely unaffected by* map3k1 *RNAi***
303 As noted above, numerous PCGs can be inhibited to cause organ duplications. However, the
304 *map3k1* RNAi phenotype described so far is largely consistent with alteration of progenitor
305 targeting behavior rather than global positional information shifting, as exemplified by the case
306 of the eye. To directly examine the spatial maintenance of positional information in *map3k1*
307 RNAi animals we labeled these animals with RNA probes for multiple PCGs. Anterior, posterior,
308 and medial PCG expression domains were largely unaffected in *map3k1* RNAi animals –
309 including expression domains for *sFRP-1, ndl-5, ndl-2, ndl-3, wntP-2, axinB,* and *slit* (Figure 5A,
310 B). The *notum*+ anterior pole, which is produced from migratory *FoxD*+ progenitors (Scimone et
311 al., 2014b), was present, but displayed some dispersal of cells, somewhat reminiscent of the
312 eye phenotype (Figure 5B). The anterior pole also displayed some disorganization during head
313 regeneration (Figure 4- figure supplement 1D). The posterior pole appeared normal (Figure 5B).
314 *axinB* transcription can serves as a read-out of the posterior-to-anterior Wnt activity gradient in
315 planarians (Iglesias et al., 2008; Reuter et al., 2015; Stückemann et al., 2017; Tewari et al.,
316 2019). *axinB* was transcribed in a similar pattern in negative control and in *map3k1* RNAi
317 animals, indicating that Wnt activity was maintained in a relatively normal spatial distribution

318 (Figure 5A). These findings are consistent with results described so far: if enough progenitors
319 can still make it to the correct TZ location, eyes will be maintained and regenerated at the
320 normal TZ, indicating positional information still remains and defines a TZ for the eye at
321 approximately the correct location in *map3k1* RNAi animals. The fact that ectopic eyes emerge
322 over time in a disordered fashion suggests that it is progenitor targeting for differentiation at
323 precise locations that is affected by *map3k1* RNAi rather than positional information.
324
325 **map3k1 *is expressed in neoblasts and migratory post-mitotic progenitors***
326 Recent scRNA-seq work has developed annotated fate-associated clusters of planarian
327 neoblasts and post-mitotic progenitors (King et al., 2024). If *map3k1* acts in progenitors to
328 regulate their differentiation, is should be transcribed in these cells. Indeed, *map3k1* transcripts
329 were present broadly across neoblast and post-mitotic progenitor clusters (Figure 5- figure
330 supplement 1), including for the eye (Figure 5- figure supplement 1C, D), neural classes
331 affected by *map3k1* RNAi (Figure 5- figure supplement 1E-G), and for the pharynx (Figure 5-
332 figure supplement 1H, I). Whereas expression data alone do not necessarily *map3k1*, these
333 data are consistent with the possibility that *map3k1* can act within migratory progenitors.
334
335 **map3k1 *is required for restricting differentiation of eye progenitors along their migratory***
336 ***path to the target zone***
337 Eye and pharynx progenitors are normally specified in restricted domains (Lapan and Reddien,
338 2011, 2012; Adler et al., 2014; Scimone et al., 2014a; Atabay et al., 2018), (referred to here as
339 progenitor specification zones). Within these domains, progenitors migrate to reach their target
340 tissue at their TZ, where they differentiate (Atabay et al., 2018; Hill and Petersen, 2018). We
341 sought to test the possibility that the ectopic differentiated cells in *map3k1* RNAi animals
342 resulted from premature progenitor differentiation at positions on their normal migratory paths,
343 before reaching the TZ. An alternative scenario we considered is that ectopic progenitor
344 specification at some distant location occurs after *map3k1* RNAi and requires excessively long-
345 range progenitor migration to reach the TZ, ultimately resulting in ectopic differentiation.
346 Planarian neoblasts can be killed with irradiation (Bardeen and Baetjer, 1904; Reddien
347 et al., 2005). Lead shielding can be utilized in X-irradiation experiments to locally protect
348 neoblasts, resulting in neoblasts present only in a restricted field (Dubois, 1948; Guedelhoefer
349 and Sánchez Alvarado, 2012; Abnave et al., 2017). Neoblasts expand only very slowly from
350 these restricted regions (barring amputation) (Saló and Baguñà, 1985), but their postmitotic
351 descendant cells serving as progenitors can readily migrate out from this region to differentiate

352 at target tissues (Guedelhoefer and Sánchez Alvarado, 2012; Abnave et al., 2017; Park et al.,
353 2023). We utilized lead shielding over the head and pre-pharyngeal region and X-irradiation to
354 preserve neoblasts only in the anterior region where eye progenitors are primarily specified
355 (Figure 6A). 48 hours after irradiation, we initiated RNAi of *map3k1* to observe the behavior of
356 any eye progenitors restricted to be born within their primary eye progenitor specification zone
357 (the zone of surviving neoblasts). 17 days after the initiation of *map3k1* RNAi, ectopic eye cells
358 and ectopic dd_17258+ neurons were apparent (Figure 6B, C). This indicates that ectopic
359 differentiation can occur after *map3k1* RNAi even from neoblasts restricted to undergo fate
360 specification close to their target tissue.
361 Second, we EdU-labeled neoblasts in *map3K1* RNAi animals after 24 days of RNAi, then
362 transplanted a pre-pharyngeal tissue fragment from these animals into the prepharyngeal region
363 of unlabeled control host animals (hosts lack *map3K1* RNAi) (Figure 6D). Animals were then
364 fixed 12 days later. This experimental design allowed assessment of the behavior of *map3k1*
365 RNAi progenitors that migrate into a non-RNAi host environment, from within the normal eye
366 progenitor specification zone. EdU-labeled cells migrated out of the transplantation region and
367 differentiated into eye cells at both the normal eye location (at the TZ) and at ectopic locations in
368 the host environment (Figure 6E). Additional ectopic eye cells were observed following
369 transplantation that were not EdU-labeled, likely the result of additional mistargeting of *map3k1*
370 RNAi progenitors from the transplant, but lacking EdU because of incomplete EdU labeling or
371 from cells born after the EdU pulse (Supplemental Figure 5A, B). These observations indicate
372 that eye progenitors originating from the normal specification zone can erroneously differentiate
373 before reaching their target location.
374
375 ***Differentiated cells in the wrong organ of* map3k1 *RNAi animals***
376 We administered *map3k1* dsRNA for RNAi and let animals undergo normal long-term tissue
377 turnover to observe the consequences of errors in progenitor targeting. We observed
378 differentiated pharynx muscle cells within the cephalic ganglia (Figure 7A). We also observed
379 other differentiated pharynx and epidermal cell types within the eye (Figure 7B), including in
380 regenerated animals (Supplemental figure 5C). These striking cell-organization defects were not
381 previously observed in the patterning phenotypes observed following RNAi of PCGs. We
382 suggest that this defect highlights the risk to tissue architecture of not enacting tight spatial
383 regulation of differentiation, especially in a biological context where progenitors are spatially
384 dispersed and migratory. Ectopic differentiated cells can become incorporated into inappropriate

385 tissue environments where they would normally never be observed, potentially disrupting tissue
386 structure and function.
387
388 **map3k1 *RNAi animals develop teratomas***
389 Long-term *map3k1* RNAi in animals undergoing tissue turnover without injury led to the
390 inevitable emergence of tissue growths (Figure 7C, D, Figure 6- figure supplement 1C). These
391 growths predominantly formed in the anterior of the animal and presented as a heterogeneous
392 collection of cell and tissue types. *vitrin*+ cells and gland cells (*mag1*) were not as common in
393 lateral outgrowths. Cell types that were present in these teratomas included eye cells, various
394 neuron types from the central nervous system (*cintillo*+, dd_17258+, dd_3524+), glia, muscle
395 cells, and *NB.22.1e* cells (Figure 7D). A similar patterning defect has been observed in
396 planarians with a defect in progenitor migration caused by *integrin* RNAi (Bonar and Petersen,
397 2017; Seebeck et al., 2017). It is known that differentiated tissues, such as the eye, can trap
398 their own progenitors and lead to their differentiation (Atabay et al., 2018; Hill and Petersen,
399 2018). This suggests that ectopic differentiation in inappropriate locations in *map3k1* RNAi
400 animals can trap more progenitors and lead to an inappropriate aggregate of differentiated cells
401 with aberrant pattern and organization. This highlights a further risk to the formation of tissue
402 architecture if the differentiation of migratory progenitors is not tightly controlled spatially.
403
404 **Discussion**
405 Planarians display continuous turnover of adult tissues through the fate specification and
406 differentiation of adult stem cells called neoblasts (Reddien, 2018). Fate specification in
407 neoblasts can occur regionally (such as in the head for eyes), but is still spatially broad and
408 intermingled. Fate-specified neoblasts (specialized neoblasts) produce progeny cells (post-
409 mitotic progenitors) that migrate to precise locations for local, highly patterned differentiation.
410 Progenitor targeting for local differentiation requires regulation from stem-cell-extrinsic signals,
411 in the form of regionally expressed genes in muscle that comprise adult planarian positional
412 information. How positional information interfaces with neoblasts and post-mitotic progenitors at
413 the molecular level to regulate migratory assortment and differentiation only at precise locations
414 is unknown and a fundamental problem of planarian regeneration and progenitor differentiation
415 regulation. We sought factors that might be required for this process through RNAi-based gene
416 perturbation experiments, and uncovered a requisite role in the spatial regulation of stem cell
417 differentiation for the *map3k1* gene, which encodes an ortholog of vertebrate MAP3K1*. map3k1*
418 RNAi animals displayed an abnormal pattern of progenitor differentiation, with differentiation

occurring in disorganized locations along post-mitotic progenitor migratory paths. We suggest a model in which *map3k1* is required for the spatial restriction of differentiation in stem cell lineages until suitable differentiation cues are encountered, either in the form of positional information (a target zone) or cues from target tissues (Figure 8A).

The defect in spatial restriction of progenitor differentiation following *map3k1* RNAi can lead to dramatic tissue patterning defects, including the differentiation of ectopic isolated cells that normally only appear in groups (e.g., isolated photoreceptor neurons), the emergence of ectopic organs, differentiated cells from one tissue type being present within an incorrect organ, and teratoma formation (Figure 8B). These tissue mispatterning attributes highlight the significance of spatial regulation of differentiation during targeting of migratory progenitors for maintaining and regenerating adult pattern. This process might prove important development in many organisms, and be particularly important in the context of adult regeneration, where tissue scale can be large and adult progenitors at least in some contexts can be challenged to migrate large distances before differentiating.

There is some differentiation of eye progenitors in the tail of *map3k1* RNAi planarians, far from the normal location of eye progenitor production and differentiation. However, only a very low rate of eye progenitor production was observed in the tail of *map3k1* RNAi animals, and a comparable low frequency of eye-specialized neoblasts were present in control tails. One interesting possibility that can be investigated in the future is that there is some noise in the spatial regulation of stem cell fate specification in planarians that does not normally contribute to errors in the spatial distribution of differentiated cells because of prevention of differentiation until cells reach their appropriate location. The progenitor specification domain for pharynx cells, by contrast, appeared to expand anteriorly after *map3k1* RNAi, indicating a possible role in the spatial regulation of progenitor specification in some cases.

Several observations suggest that the defects in targeting in *map3k1* RNAi animals involves a process within the neoblasts and their post-mitotic progenitor descendants, rather than in a role for *map3k1* in establishing the progenitor-extrinsic cues (e.g., muscle PCGs) that facilitate progenitor targeting. First, PCG expression patterns themselves were largely normal following *map3k1* RNAi. Second, ectopic differentiation after *map3k1* RNAi was more spatially disorganized than is observed for patterning phenotypes that occur following the shifting of PCG coordinates (such as a posterior line of ectopic eyes in *ndk* RNAi animals (Cebria et al., 2002) or a lateral line of ectopic eyes in *wnt5* RNAi animals (Atabay et al., 2018)). Third, ectopic cells following *map3k1* RNAi were frequently isolated, as opposed to appearing exclusively in organized aggregates or forming ectopically placed organs. Fourth, transplantation of EdU-

453 labeled tissue grafts from *map3k1* RNAi animals into the pre-pharyngeal region of control
454 animals showed instances of ectopic differentiation in wild-type host tissue. Finally, during
455 regeneration or following eye resection, progenitors can still be targeted to the correct target
456 zone for the eye, indicating that the eye target zone still remains after *map3k1* RNAi. One
457 possibility is that Map3k1 applies a brake on differentiation in progenitors that is released or
458 overcome by some cue associated with a progenitor reaching its target zone or by interacting
459 with its target tissue.

460 Map kinase signaling cascades are versatile pathway modules found throughout the
461 animal kingdom and are involved in diverse processes (Widmann et al., 1999). The kinases and
462 accompanying cofactors in these modules enable the regulated activation of various Map
463 kinases (e.g., ERK1/2, p38, JNK) (Suddason and Gallagher, 2015). Map kinase kinase kinases
464 (MAP3Ks) are one of the first activated proteins in these cascades, often responding to receptor
465 tyrosine kinase signaling at the cell membrane. In mammals, there are 24 characterized
466 MAP3Ks: MAP3K1 through MAP3K21, B-Raf, C-Raf, and A Raf, which activate downstream
467 MAP2K proteins through phosphorylation. Among the MAP3K proteins, MAP3K1 is unique in its
468 domain composition. In particular, MAP3K1 orthologs are the only MAP3K with a PHD domain
469 (Suddason and Gallagher, 2015). The MAP3K1 domain architecture enables a role in
470 ubiquitination as well as kinase activity (Pham et al., 2013). In mammals, *map3k1* has a role in
471 regulating many processes such as proliferation, differentiation, division, and cell death
472 (Suddason and Gallagher, 2015). *map3k1* gene functions are not well characterized in most
473 invertebrate systems, and *Drosophila* and *C. elegans* have no identified *map3k1* orthologs
474 (Widmann et al., 1999). Planarians therefore present an attractive invertebrate model for
475 dissection of *map3k1* function. There is evidence for the role of various Map-kinases (e.g., ERK,
476 MEK, RAS, p38) in planarian regeneration, particularly in the blastema formation and the wound
477 and missing tissue response programs (Tasaki et al., 2011a; Tasaki et al., 2011b; Owlarn et al.,
478 2017; Wang et al., 2020). *map3k1* has been studied in a different planarian species, *D. japonica*
479 (Hosoda et al., 2018). This work suggested a possible role for *map3k1* in the scaling and
480 patterning of the trunk and head regions of regenerating animals, proposed to be through
481 alternation of ERK and β-catenin gradients (Hosoda et al., 2018). Additionally, *map3k1* has
482 been implicated in germ cell proliferation and terminal differentiation of stem cells in the parasitic
483 flatworm *E. multilocularis* through JNK signaling (Stoll et al., 2021). It will be of interest to further
484 dissect the molecular role of *map3k1* in planarian progenitor differentiation, and to determine
485 whether *map3k1* orthologs have similar roles in regulating differentiation in additional
486 regenerative organisms.

487 Adult patterning systems in some organisms can rely on a spatially coarse progenitor
488 specification system, migratory assortment of progenitors, and local differentiation. This process
489 involves progenitor transitions from spatially broad and disorganized, to local and highly
490 patterned as cells transit from stem cell to post-mitotic migratory progenitor. This suggests that
491 regulation of terminal differentiation must have a central role in pattern production. Progenitor-
492 extrinsic positional information has a prominent regulatory role in this process, and some
493 mechanism(s) could exist within the progenitors themselves to enable spatial restriction of
494 differentiation until suitable cues have been received. We suggest that *map3k1* acts within
495 planarian progenitors to mediate such spatial restriction on differentiation, and that this is critical
496 for preventing mistargeting differentiation to the incorrect location or organ, and to prevent
497 teratoma formation.
498

499 **Acknowledgements**
500 The authors thank members of the Reddien lab for helpful comments and discussion.
501 We acknowledge support from NIH R35 GM145345. PWR is an investigator of HHMI and an
502 associate member of the Broad Institute. We thank the Eleanor Schwartz Charitable Foundation
503 for support.
504

505 **Materials and methods**
506

507 **Animal husbandry and surgery**
508 Asexual *S. mediterranea* clonal strain CIW4 was used for all experiments. Animals were
509 cultured in static 1x Montjuic water (1.6 mmol/l NaCl, 1.0 mmol/l $CaCl_2$, 1.0 mmol/l $MgSO_4$, 0.1
510 mmol/l $MgCl_2$, 0.1 mmol/l KCl and 1.2 mmol/l $NaHCO_3$ prepared in Milli-Q water) at 20°C.
511 Amputations were performed under cold conditions (~4C) with a scalpel. Animals were fed
512 homogenized beef liver weekly, with water changed biweekly. Animals were starved for
513 approximately seven days before experiments.
514

515 **Whole-mount fluorescent in situ hybridization (FISH)**
516 Animal mucus was removed using 5% N-acetylcysteine in PBS; animals were then fixed with
517 4% formaldehyde in PBST for 20 minutes, with rocking. Animals were then washed with PBST,
518 incubated in 1:1 PBST:methanol, then stored in 100% methanol at -20C until ready for
519 bleaching. Animals were moved into mesh baskets in a 24-well plate where all remaining steps
520 were carried out. Animals were placed on a light source to bleach for 1.5 hours in a bleaching

521 solution (5% formamide, 0.5x SSC, and 1.2% hydrogen peroxide). After 2 PBST washes,
522 animals were then treated with 5 mg/ml Proteinase K for 10 minutes, followed by 4%
523 formaldehyde post-fixation in PBST.
524
525 RNA probes were transcribed using DIG, FITC, or DNP-modified nucleotides, allowing signal
526 amplification through the use of DIG, FITC, and DNP antibodies conjugated to an HRP. Probes
527 were diluted in Hybe solution (1:800) (50% deionized formamide, 5x SSC, 1 mg/mL yeast RNA,
528 1% Tween-20, 5% dextran sulfate), and left to incubate overnight. The following days, we
529 performed antibody incubations at 4C overnight using anti-DIG-POD (1:1500, Roche; 10%
530 western blocking solution (Roche)), anti-FITC-POD (1:2,000, Roche; 5% horse serum, 5%
531 western blocking solution), and anti-DNP-HRP (1:100, Perkin-Elmer; blocking solution with 10%
532 inactivated Horse Serum). Tyramide signal amplification involved incubating in rhodamine
533 (1:1,000), fluorescein (1:1,500), or Cy5 (1:300) in borate buffer (0.1M boric acid, 2M NaCl, pH
534 8.5) containing 0.0003% hydrogen peroxide for 10 minutes. Samples were incubated in 1%
535 sodium azide for 2 hours to inactivate the HRP. Blocking and antibody incubations then
536 occurred for detection of the second probe. Animals were incubated overnight in 1mg/mL DAPI
537 solution at 4C. Animals were mounted on coverslips in ProLong Gold Antifade Mountant
538 (Thermo Fisher).
539
540 **EdU labeling and detection**
541 F-ara-EdU (Click Chemistry Tools) was diluted in Dimethyl sulfoxide (DMSO) to 200mg/ml, then
542 diluted in static 1x Montjuic water to 1.25mg/mL. Animals were split into 10 animals per well in a
543 12-well plate, then soaked in 1.25mg/mL EdU solution for 20 hours following 1 week of
544 starvation. EdU solution was replaced with 5mg/mL Instant Ocean sea salt dissolved in Milli-Q
545 water. Prior to probe hybridization in the *in situ* hybridization protocol, following proteinase K
546 and 4% formaldehyde incubations, cells were incubated in a “click reaction”- 1% 100 mM
547 CuSO4, 0.1% 10 mM TAMRA-Azide-fluor 545 (Sigma-Aldrich), and 20% 50 mM ascorbic acid in
548 PBS- for 30 minutes in the dark, proceeded by 6 PBST washes and continuation of the probe
549 hybridization step.
550
551 **RNA interference**
552 dsRNA for RNAi was prepared using in vitro transcription with T7 polymerase (Promega).
553 Template was generated with PCR; primers contained T7 promoters. RNA was resuspended in

554 water and dsRNA annealed. *C. elegans unc-22* dsRNA was used as the negative control for all
555 RNAi experiments.
556
557 **Transplantation**
558 EdU plug transplants were performed using *map3k1* RNAi animals, 12 hours following a 20 hour
559 EdU pulse, as the donor to a recipient wild type animal. Donor animals were anesthetized with
560 0.2% chlorotone solution, followed by an incubation in Holfreter's solution, then placed on an ice
561 block covered in Whatman filter paper moistened with 1x Montjuic water to surgically manipulate
562 with a clean scalpel. EdU+ *map3k1* RNAi donor animals and wild type recipients both had a
563 center portion of their pre-pharyngeal regions removed. The pre-pharyngeal donor graft from the
564 *map3k1* RNAi animal was placed in the EdU- wild type recipient's pre-pharyngeal region.
565 Recipients were then gently covered with cigarette paper soaked in chilled Holfreter's solution
566 and transferred to a small petri dish with just enough Holfreter's solution to cover the bottom of
567 the dish. Animals were put at 10C for 20 hours; the following day, transplant recipients were
568 gently recovered and put into 1x Montjuic water containing .1% gentamicin (Gibco).
569
570 **Shielded irradiation**
571 Animals were irradiated using a Gammacell-40 137-cesium source. For shielded irradiation
572 experiments, animals were anesthetized with 0.2% chlorotone, then arranged on Whatman filter
573 paper in a petri dish sitting on ice. Animals were oriented to have their anterior half covered by
574 the lead shield placed over the petri dish. Samples were placed in a Gammacell chamber and
575 exposed to 3000 Rad of unidirectional X-irradiation. Animals were rescued with 1x Montjuic
576 water and stored in 1x Montjuic water with .1% gentamicin (Gibco) until further experimentation.
577
578 **Image analysis and statistical analysis**
579 For cell counts, the AP axis was binned into 6 regions according to anatomical landmarks. AP_1
580 (head tip to bottom of brain), AP_2 (bottom of brain to top of pharynx), AP_3 (top of pharynx to
581 middle of pharynx), AP_4 (middle of pharynx to bottom of pharynx), AP_5 (top half of the tail)
582 and AP_6 (bottom half of the tail). Each animal had one data point for each of the 6 bins.
583 Graphpad Prism software was used for graph generation and statistical analysis using a Mann-
584 Whitney-U test with a significance cut off of p=.05. For cell count comparisons in the tail,
585 Graphpad Prism software was used for graph generation and statistical analysis using a student
586 t-test with a significance cut off of p=.05.
587

References

Abnave, P., Aboukhatwa, E., Kosaka, N., Thompson, J., Hill, M.A., and Aboobaker, A.A. (2017). Epithelial-mesenchymal transition transcription factors control pluripotent adult stem cell migration in vivo in planarians. Development *144*, 3440-3453.

Adler, C.E., Seidel, C.W., McKinney, S.A., and Sánchez Alvarado, A. (2014). Selective amputation of the pharynx identifies a *FoxA*-dependent regeneration program in planaria. Elife *3*, e02238.

Atabay, K.D., LoCascio, S.A., de Hoog, T., and Reddien, P.W. (2018). Self-organization and progenitor targeting generate stable patterns in planarian regeneration. Science *360*, 404-409.

Bardeen, C.R., and Baetjer, F.H. (1904). The inhibitive action of the Roentgen rays on regeneration in planarians. J Exp Zool *1*, 191-195.

Bonar, N.A., and Petersen, C.P. (2017). Integrin suppresses neurogenesis and regulates brain tissue assembly in planarian regeneration. Development *144*, 784-794.

Cebria, F., Kobayashi, C., Umesono, Y., Nakazawa, M., Mineta, K., Ikeo, K., Gojobori, T., Itoh, M., Taira, M., Sánchez Alvarado, A.*, et al.* (2002). FGFR-related gene nou-darake restricts brain tissues to the head region of planarians. Nature *419*, 620-624.

Cebria, F., and Newmark, P.A. (2007). Morphogenesis defects are associated with abnormal nervous system regeneration following roboA RNAi in planarians. Development *134*, 833-837.

Dubois, F. (1948). Démostration de la migration des cellules de régénération des planaries par le méthode des greffes et des irradiations combinées. Séance, 1316-1318.

Eisenhoffer, G.T., Kang, H., and Sánchez Alvarado, A. (2008). Molecular analysis of stem cells and their descendants during cell turnover and regeneration in the planarian *Schmidtea mediterranea*. Cell Stem Cell *3*, 327-339.

Fincher, C.T., Wurtzel, O., de Hoog, T., Kravarik, K.M., and Reddien, P.W. (2018). Cell type transcriptome atlas for the planarian *Schmidtea mediterranea*. Science *360*, 874.

Guedelhoefer, O.C., and Sánchez Alvarado, A. (2012). Amputation induces stem cell mobilization to sites of injury during planarian regeneration. Development.

Gurley, K.A., Elliott, S.A., Simakov, O., Schmidt, H.A., Holstein, T.W., and Sánchez Alvarado, A. (2010). Expression of secreted Wnt pathway components reveals unexpected complexity of the planarian amputation response. Dev Biol *347*, 24-39.

Hill, E.M., and Petersen, C.P. (2015). Wnt/Notum spatial feedback inhibition controls neoblast differentiation to regulate reversible growth of the planarian brain. Development *142*, 4217-4229.

Hill, E.M., and Petersen, C.P. (2018). Positional information specifies the site of organ regeneration and not tissue maintenance in planarians. Elife *7*.

Hosoda, K., Motoishi, M., Kunimoto, T., Nishimura, O., Hwang, B., Kobayashi, S., Yazawa, S., Mochii, M., Agata, K., and Umesono, Y. (2018). Role of MEKK1 in the anterior-posterior patterning during planarian regeneration. Dev Growth Differ *60*, 341-353.

Hyman, L.H. (1951). The Invertebrates: Platyhelminthes and Rhynchocoela The acoelomate bilateria, Vol II (New York: McGraw-Hill Book Company Inc.).

634 Iglesias, M., Gomez-Skarmeta, J.L., Saló, E., and Adell, T. (2008). Silencing of *Smed-*
635 *betacatenin1* generates radial-like hypercephalized planarians. Development *135*, 1215-
636 1221.
637 King, H.O., Owusu-Boaitey, K.E., Fincher, C.T., and Reddien, P.W. (2024). A
638 transcription factor atlas of stem cell fate in planarians. Cell Rep *43*, 113843.
639 Kobayashi, C., Saito, Y., Ogawa, K., and Agata, K. (2007). Wnt signaling is required for
640 antero-posterior patterning of the planarian brain. Dev Biol *306*, 714-724.
641 Lapan, S.W., and Reddien, P.W. (2011). *dlx* and *sp6-9* control optic cup regeneration in
642 a prototypic eye. PLoS Genet *7*, e1002226.
643 Lapan, S.W., and Reddien, P.W. (2012). Transcriptome Analysis of the Planarian Eye
644 Identifies *ovo* as a Specific Regulator of Eye Regeneration. Cell Reports *2*, 294-307.
645 Li, D.J., McMann, C.L., and Reddien, P.W. (2019). Nuclear receptor NR4A is required
646 for patterning at the ends of the planarian anterior-posterior axis. Elife *8*.
647 Oderberg, I.M., Li, D.J., Scimone, M.L., Gavino, M.A., and Reddien, P.W. (2017).
648 Landmarks in Existing Tissue at Wounds Are Utilized to Generate Pattern in
649 Regenerating Tissue. Curr Biol *27*, 733-742.
650 Owlarn, S., Klenner, F., Schmidt, D., Rabert, F., Tomasso, A., Reuter, H., Mulaw, M.A.,
651 Moritz, S., Gentile, L., Weidinger, G.*, et al.* (2017). Generic wound signals initiate
652 regeneration in missing-tissue contexts. Nature Commun *8*, 2282.
653 Park, C., Owusu-Boaitey, K.E., Valdes, G.M., and Reddien, P.W. (2023). Fate
654 specification is spatially intermingled across planarian stem cells. Nature
655 communications *14*, 7422.
656 Pham, T.T., Angus, S.P., and Johnson, G.L. (2013). MAP3K1: Genomic Alterations in
657 Cancer and Function in Promoting Cell Survival or Apoptosis. Genes Cancer *4*, 419-
658 426.
659 Plass, M., Solana, J., Wolf, F.A., Ayoub, S., Misios, A., Glazar, P., Obermayer, B.,
660 Theis, F.J., Kocks, C., and Rajewsky, N. (2018). Cell type atlas and lineage tree of a
661 whole complex animal by single-cell transcriptomics. Science *360*, 875.
662 Reddien, P.W. (2018). The Cellular and Molecular Basis for Planarian Regeneration.
663 Cell *175*, 327-345.
664 Reddien, P.W. (2022). Positional Information and Stem Cells Combine to Result in
665 Planarian Regeneration. Cold Spring Harb Perspect Biol *14*.
666 Reddien, P.W., Oviedo, N.J., Jennings, J.R., Jenkin, J.C., and Sánchez Alvarado, A.
667 (2005). SMEDWI-2 is a PIWI-like protein that regulates planarian stem cells. Science
668 *310*, 1327-1330.
669 Reuter, H., Marz, M., Vogg, M.C., Eccles, D., Grifol-Boldu, L., Wehner, D., Owlarn, S.,
670 Adell, T., Weidinger, G., and Bartscherer, K. (2015). Beta-catenin-dependent control of
671 positional information along the AP body axis in planarians involves a teashirt family
672 member. Cell Rep *10*, 253-265.
673 Saló, E., and Baguñà, J. (1985). Cell movement in intact and regenerating planarians.
674 Quantitation using chromosomal, nuclear and cytoplasmic markers. J Embryol Exp
675 Morphol *89*, 57-70.
676 Scimone, M.L., Cote, L.E., Rogers, T., and Reddien, P.W. (2016). Two FGFRL-Wnt
677 circuits organize the planarian anteroposterior axis. Elife *5*.

678 Scimone, M.L., Kravarik, K.M., Lapan, S.W., and Reddien, P.W. (2014a). Neoblast
679 Specialization in Regeneration of the Planarian *Schmidtea mediterranea*. Stem Cell
680 Reports *3*, 339-352.
681 Scimone, M.L., Lapan, S.W., and Reddien, P.W. (2014b). A *forkhead* transcription
682 factor is wound-induced at the planarian midline and required for anterior pole
683 regeneration. PLoS genetics *10*, e1003999.
684 Seebeck, F., Marz, M., Meyer, A.W., Reuter, H., Vogg, M.C., Stehling, M., Mildner, K.,
685 Zeuschner, D., Rabert, F., and Bartscherer, K. (2017). Integrins are required for tissue
686 organization and restriction of neurogenesis in regenerating planarians. Development
687 *144*, 795-807.
688 Stoll, K., Bergmann, M., Spiliotis, M., and Brehm, K. (2021). A MEKK1 - JNK mitogen
689 activated kinase (MAPK) cascade module is active in *Echinococcus multilocularis* stem
690 cells. PLoS Negl Trop Dis *15*, e0010027.
691 Stückemann, T., Cleland, J.P., Werner, S., Thi-Kim Vu, H., Bayersdorf, R., Liu, S.Y.,
692 Friedrich, B., Julicher, F., and Rink, J.C. (2017). Antagonistic Self-Organizing Patterning
693 Systems Control Maintenance and Regeneration of the Anteroposterior Axis in
694 Planarians. Dev Cell *40*, 248-263 e244.
695 Suddason, T., and Gallagher, E. (2015). A RING to rule them all? Insights into the
696 Map3k1 PHD motif provide a new mechanistic understanding into the diverse roles of
697 Map3k1. Cell Death Differ *22*, 540-548.
698 Tasaki, J., Shibata, N., Nishimura, O., Itomi, K., Tabata, Y., Son, F., Suzuki, N., Araki,
699 R., Abe, M., Agata, K.*, et al.* (2011a). ERK signaling controls blastema cell
700 differentiation during planarian regeneration. Development *138*, 2417-2427.
701 Tasaki, J., Shibata, N., Sakurai, T., Agata, K., and Umesono, Y. (2011b). Role of c-Jun
702 N-terminal kinase activation in blastema formation during planarian regeneration. Dev
703 Growth Differ *53*, 389-400.
704 Tewari, A.G., Owen, J.H., Petersen, C.P., Wagner, D.E., and Reddien, P.W. (2019). A
705 small set of conserved genes, including *sp5* and *Hox*, are activated by Wnt signaling in
706 the posterior of planarians and acoels. PLoS Genet *15*, e1008401.
707 van Wolfswinkel, J.C., Wagner, D.E., and Reddien, P.W. (2014). Single-Cell Analysis
708 Reveals Functionally Distinct Classes within the Planarian Stem Cell Compartment. Cell
709 Stem Cell *15*, 326-339.
710 Wang, Q., Liu, Y., Jin, B., Dong, Z., Chen, G., and Liu, D. (2020). *Djmek* is involved in
711 planarian regeneration by regulation of cell proliferation and apoptosis. Biochem
712 Biophys Res Commun *532*, 355-361.
713 Wenemoser, D., and Reddien, P.W. (2010). Planarian regeneration involves distinct
714 stem cell responses to wounds and tissue absence. Dev Biol *344*, 979-991.
715 Widmann, C., Gibson, S., Jarpe, M.B., and Johnson, G.L. (1999). Mitogen-activated
716 protein kinase: conservation of a three-kinase module from yeast to human. Physiol Rev
717 *79*, 143-180.
718 Witchley, J.N., Mayer, M., Wagner, D.E., Owen, J.H., and Reddien, P.W. (2013).
719 Muscle cells provide instructions for planarian regeneration. Cell Reports *4*, 633-641.
720 Zeng, A., Li, H., Guo, L., Gao, X., McKinney, S., Wang, Y., Yu, Z., Park, J., Semerad,
721 C., Ross, E.*, et al.* (2018). Prospectively Isolated Tetraspanin(+) Neoblasts Are Adult
722 Pluripotent Stem Cells Underlying Planaria Regeneration. Cell *173*, 1593-1608 e1520.

723 Zhu, S.J., Hallows, S.E., Currie, K.W., Xu, C., and Pearson, B.J. (2015). A *mex3*
724 homolog is required for differentiation during planarian stem cell lineage development.
725 eLife *4*.
726
727

728 **Figure legends**

729

730 **Figure 1. *map3k1* RNAi results in ectopic eyes and ectopic isolated eye cells. A.** Live
731 images (upper panels) showing posterior eyes in *map3k1* RNAi animals. Upper panels, 6
732 feedings of RNAi over 36 days. FISH (bottom panels): single optic cup and photoreceptor cells
733 are present ectopically with RNA probes for *opsin* (photoreceptors), a *catalase/tyrosinase/glut3*
734 pool (optic cup), and an anti-Arrestin antibody (labeling photoreceptors and their projections). **B.**
735 Examples showing a diversity of ectopic eyes and eye cells in *map3k1* RNAi animals. **A, B.**
736 Dorsal up; Scale bar, 200μm. **C.** Schematic comparing previously identified eye-patterning
737 phenotypes with the *map3k1* RNAi phenotype. **D.** FISH of single cells differentiated proximal to
738 the pharynx and in the tail of *map3k1* RNAi animals. Dorsal up; scale bar, 100μm. **E.** FISH
739 examples of *ovo*+; *smedwi-1*+ cells in the tail. **F.** Left graph depicts the number of ectopic optic
740 cup differentiation events per animal along the AP axis over 10, 16, and 26 days. Right graph
741 depicts the number of ectopic photoreceptor neurons at 26 days of *map3k1* RNAi; See also
742 Figure 1- figure supplement 1.

743

744 **Figure 2. *map3k1* RNAi results in ectopic neuron classes and gland cells along the AP**
745 **axis. A.** *map3k1* RNAi animals exhibit posterior ectopic brain branches with *chat*+ neurons and
746 *gluR*+ (dd_16476) neurons. Photoreceptor axons extend along ventral nerve cords and into
747 ectopic brain branches. Ventral up; Scale bars, 200μm; Closeup images, scale bar, 100μm. **B.**
748 FISH images showing no change in *cintillo*+ neuron distribution, but expansion of dd_17258+
749 cells down the entire AP axis. ventral up; scale bars, 200μm; See also Figure 2- figure
750 supplement 1. **C.** Graph showing distribution of dd_17258+ cells along the AP axis in control
751 and *map3k1* RNAi animals. **D.** Quantification of cells in the tail for dd_7131 and dd_8476. More
752 cells are observed in the tails of *map3k1* RNAi animals compared to control animals; Student t-
753 test using Graphpad Prism software ***p<.0001; **p<.001 . **E.** FISH examples of unaffected
754 (dd_9223) and affected (dd_7131 and dd_8476) parenchymal cell types in *map3k1* RNAi
755 animals. ventral up; scale bar, 200μm. Numbers of animals are represented on the bottom left of
756 each panel.

757

758 **Figure 3. *map3k1* RNAi results in pharynx cell types in ectopic anterior locations. A.** FISH
759 images showing anterior expansion and disorganization of *vitrin*+ (pharynx-specific marker)
760 cells along the AP-axis. Ventral up; scale bars, 100μm. **B.** FISH showing anterior expansion of
761 *NB.22.1e* (mouth and esophagus) cells along the AP axis. *map3k1* RNAi animals exhibit a low

762 frequency of *NB.22.1e* cells in the tail, posterior to the normal mouth location. **C.** FISH shows
763 anterior expansion of *mhc1*+ cells in *map3k1* RNAi animals compared to control animals.
764 ventral up, scale bar, 100µm. **D.** FISH shows anterior expansion of dd_554 cells (pharynx
765 progenitors) in *map3k1* RNAi animals compared to control animals. Ventral, up. Scale bar,
766 100µm. **E.** FISH shows *FoxA*+; *smedwi-1*+ cells close to the brain lobes and eyes. Scale bar,
767 50µm.
768
769 **Figure 4. *map3k1* RNAi animals display tissue-specific regeneration at target zones. A.**
770 Top, schematic depicts experimental design. Bottom panels show live image examples of
771 control and *map3k1* RNAi animal eye resections at d0, d1, and d10 post eye resection. Scale
772 bar, 200µm. **B.** Diagram, pharynx resection. Control and *map3k1* RNAi animals at d1 and d10
773 post resection; accompanied by FISH of d10 pharynx regeneration using probes to *vitrin*
774 (pharynx-specific), *NB.22.1e* (mouth and esophagus), and *mhc1* (pharynx muscle). Scale bar,
775 200µm**;** See also Figure 4- figure supplement 1. **C.** d10 regeneration in head, trunk, and tail
776 fragments. An anterior-shifted pharynx regenerated in a *map3k1* RNAi tail fragment. Scale bar,
777 200µm**. D.** FISH images of d10 trunk and tail regenerates showing regeneration of
778 photoreceptors (anti-Arrestin), pharynx (*vitrin*), and mouth and esophagus (*NB.22.1e*). An
779 anterior shift in *vitrin*+ cells in d10 tail regenerate. Scale bar, 200µm. **E.** AP distributions of
780 original trunk pharynges in control and *map3k1* RNAi animals and ectopic differentiation events
781 in *map3k1* RNAi trunk regenerates **** p <.0001 Mann-Whitney-U test. **F.** AP distributions of
782 regenerated pharynges in tail fragments shows an anterior shift in pharynx regeneration in
783 *map3k1* RNAi animals compared to control animals. *** p <.0001 Mann-Whitney-U test.
784
785 **Figure 5. Positional information remains largely unaffected in *map3k1* RNAi animals**
786 **A.** FISH panel of position control genes (*sFRP-1, ndl2, ndl5, ndl3, wntP-2, axinB, and slit*)
787 shows no obvious changes to positional information. Sample numbers are indicated in the lower
788 left of each panel. Scale bar, 200µm. **B.** FISH showing some dispersion of *notum*+ cells in the
789 heads of *map3k1* RNAi animals compared to control animals. Right panels, no obvious changes
790 in posterior pole organization. Sample numbers are indicated in the lower left of each panel,
791 scale bars, 200µm.
792
793 **Figure 6. *map3k1* RNAi eye progenitors prematurely differentiate along their typical**
794 **migratory path. A.** Schematic of head-shielded irradiation experimental design. **B.** FISH
795 showing instances of ectopic photoreceptor (anti-Arrestin), optic cup (*catalase, tyrosinase,*

796 *glut3*), and dd_17258 cells born in the upper half of the animal (n=3/3 with good shielding and
797 cells present correspond to area of leftover neoblasts). **C.** Schematic of EdU-labeled transplant
798 experimental design. **D.** FISH and antibody staining showing examples of EdU+ eye cells from
799 *map3k1* RNAi animals ectopically differentiated in wild-type animals (n=7/18 with EdU+ ectopic
800 cells; n=16/18 exhibiting any ectopic eye cells outside the transplant area). Scale bar, 50μm.
801
802 **Figure 7. *map3k1* RNAi results in differentiation in incorrect organs and teratoma**
803 **formation. A.** FISH of long term (>6 weeks) *map3k1* RNAi animal showing clusters of *mhc1*
804 cells that appear to have formed small structures within the lobes of the brain and ventral cords.
805 Right panels depict *NB.22.1e* cells incorporated into the eye (anti-Arrestin). Number of animals
806 analyzed is indicated in the lower left of each panel; Left panel scale bar, 200μm; all other
807 panels scale bars, 50μm. **B.** FISH showing *vitrin*+ cells incorporated into the eyes of a d10 tail
808 regenerate. n=9/24 animals contained at least one *vitrin*+ cell in one eye; left panels scale bar,
809 200μm. All other scale bars, 50μm. **C.** Left panel contains live images of early developing
810 growths in *map3k1* RNAi animals, accompanied by a DAPI image of an outgrowth in between
811 the brain lobes. Scale bars 200μm; The right panel contains live images and FISH examples of
812 late-stage teratomas from *map3k1* RNAi animals between 12 and 16 feedings, accompanied by
813 FISH examples showing eyes dispersed around the teratomas. Scale bars, 200μm. **D.** Left
814 panels are FISH images showing an exclusion of *vitrin*+ cells from lateral outgrowths but a
815 common presence of *NB.22.1e*+ cells in outgrowths. *mag1*, a parenchymal marker with
816 transcripts abundant in cells in the neck region is also mostly excluded from outgrowths. Right
817 panel shows examples of cell types commonly found in outgrowths: *cintillo* (neuron), dd_17258
818 (neuron), dd_3534 (neuron), *estrella* (glia), anti-Arrestin (photoreceptor projections), *NB.22.1e*,
819 *lamin* (mouth, epidermis), and *col2* (muscle). Scale bar 100μm.
820
821 **Figure 8. Model: Map3K1 restricts migratory progenitor differentiation until they reach**
822 **their target. A.** Schematic showing the inhibition of differentiation of a specific progenitor until
823 reaching its target tissue at the target zone. **B.** Defects observed with *map3k1* RNAi,
824 highlighting significance of restricting differentiation until suitable contextual cues are reached.
825

Figure 1

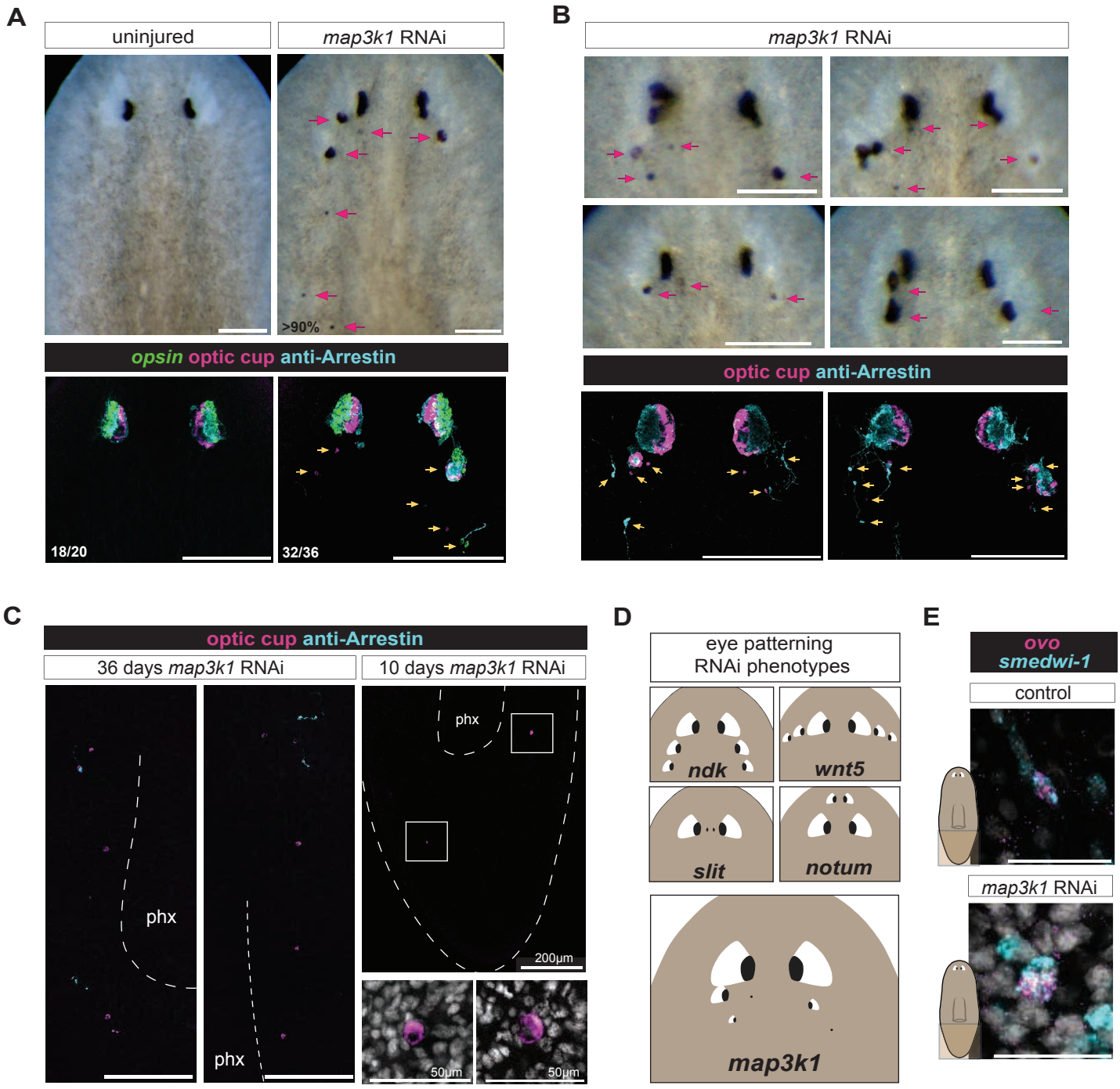
A
uninjured
map3k1 RNAi
>90%
opsin optic cup anti-Arrestin
18/20
32/36
B
map3k1 RNAi
optic cup anti-Arrestin
C
optic cup anti-Arrestin
36 days map3k1 RNAi
10 days map3k1 RNAi
phx
phx
phx
200µm
50µm
50µm
D
eye patterning
RNAi phenotypes
ndk
wnt5
slit
notum
map3k1
E
ovo
smedwi-1
control
map3k1 RNAi

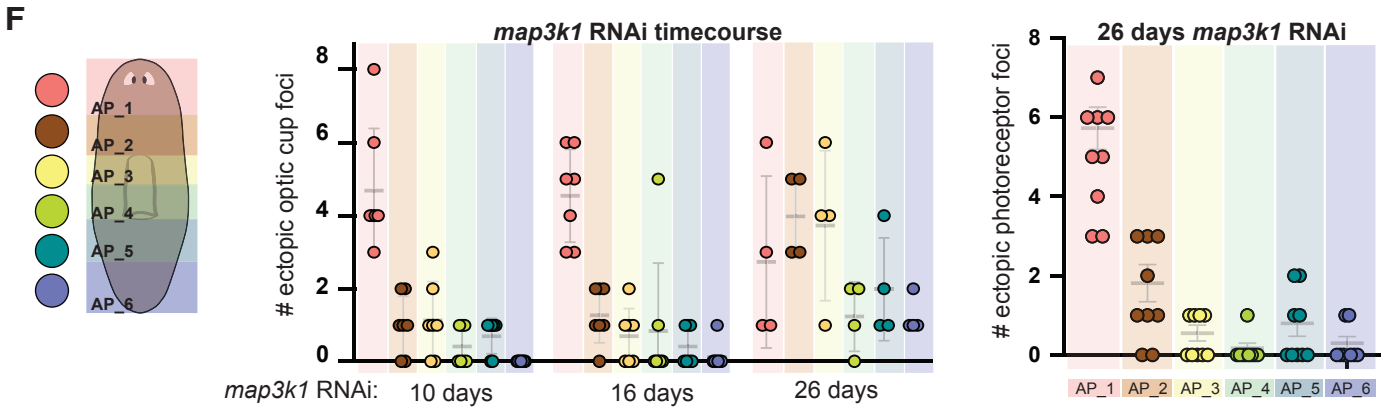
F
AP_1
AP_2
AP_3
AP_4
AP_5
AP_6
map3k1 RNAi timecourse
ectopic optic cup foci
0
2
4
6
8
map3k1 RNAi:
10 days
16 days
26 days
26 days map3k1 RNAi
ectopic photoreceptor foci
AP_1
AP_2
AP_3
AP_4
AP_5
AP_6

Figure 2

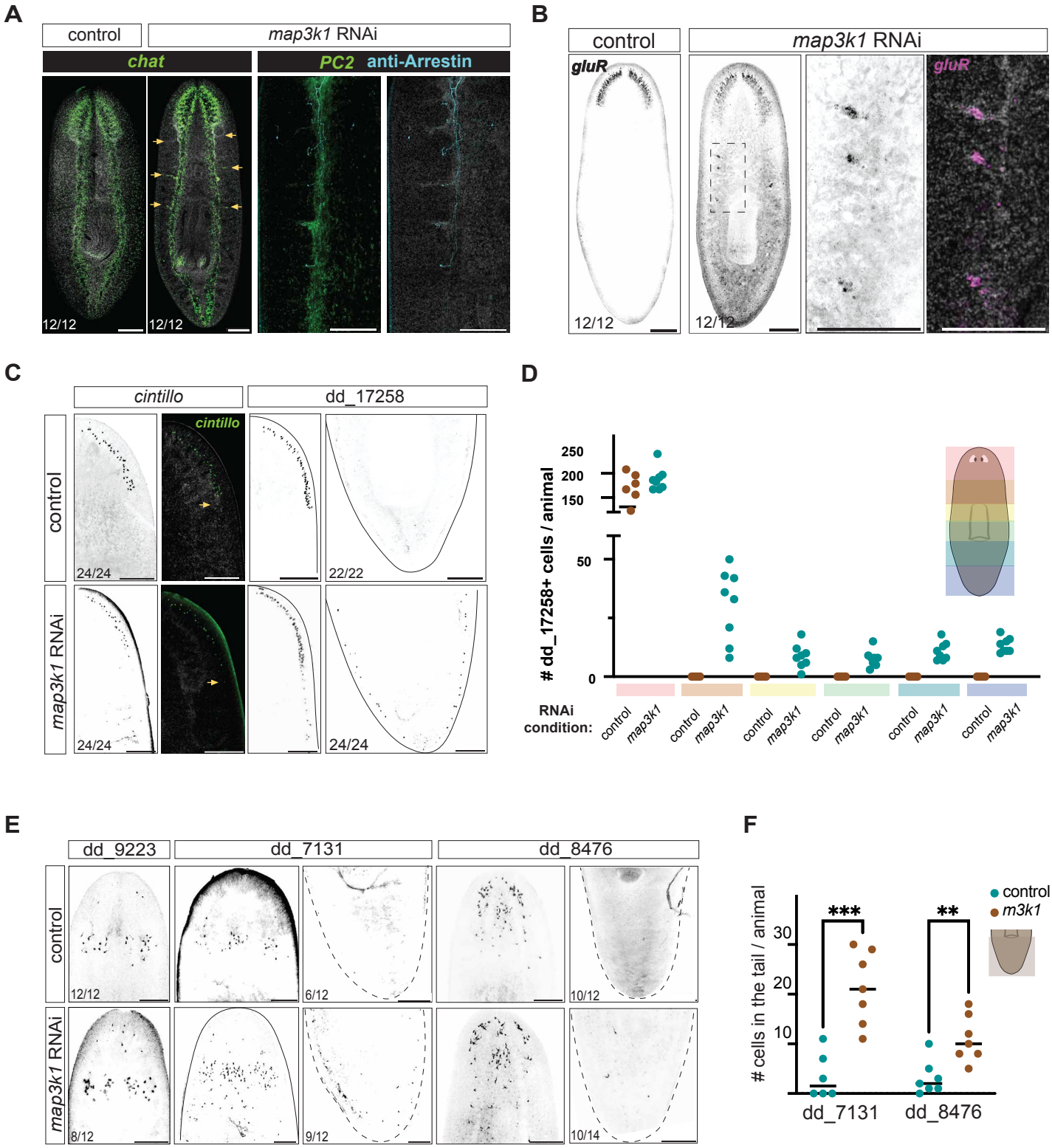
A
control
map3k1 RNAi
chat
PC2
anti-Arrestin
12/12
12/12
B
control
map3k1 RNAi
gluR
gluR
12/12
12/12
C
cintillo
dd_17258
control
map3k1 RNAi
cintillo
24/24
22/22
24/24
24/24
D
dd_17258+ cells / animal
250
200
150
50
0
RNAi condition:
control
map3k1
E
dd_9223
dd_7131
dd_8476
control
map3k1 RNAi
12/12
6/12
10/12
8/12
9/12
10/14
F
cells in the tail / animal
control
m3k1
***
**
30
20
10
dd_7131
dd_8476

Figure 3

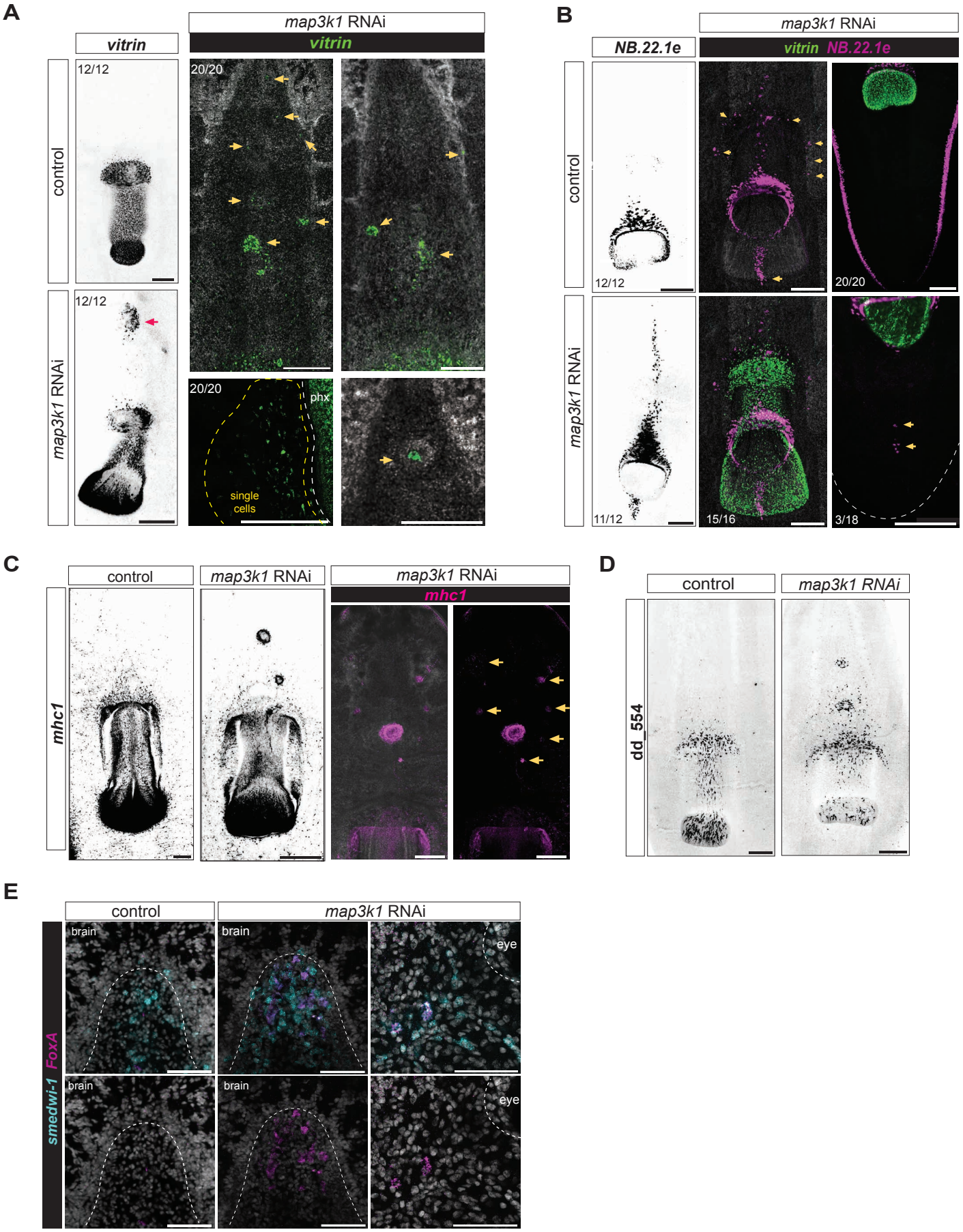
A
vitrin
map3k1 RNAi
vitrin
control
map3k1 RNAi
12/12
12/12
20/20
20/20
phx
single cells
B
NB.22.1e
map3k1 RNAi
vitrin NB.22.1e
control
map3k1 RNAi
12/12
20/20
11/12
15/16
3/18
C
control
map3k1 RNAi
map3k1 RNAi
mhc1
mhc1
D
control
map3k1 RNAi
dd_554
E
control
map3k1 RNAi
smedwi-1 FoxA
brain
brain
eye
brain
brain
eye

Figure 4

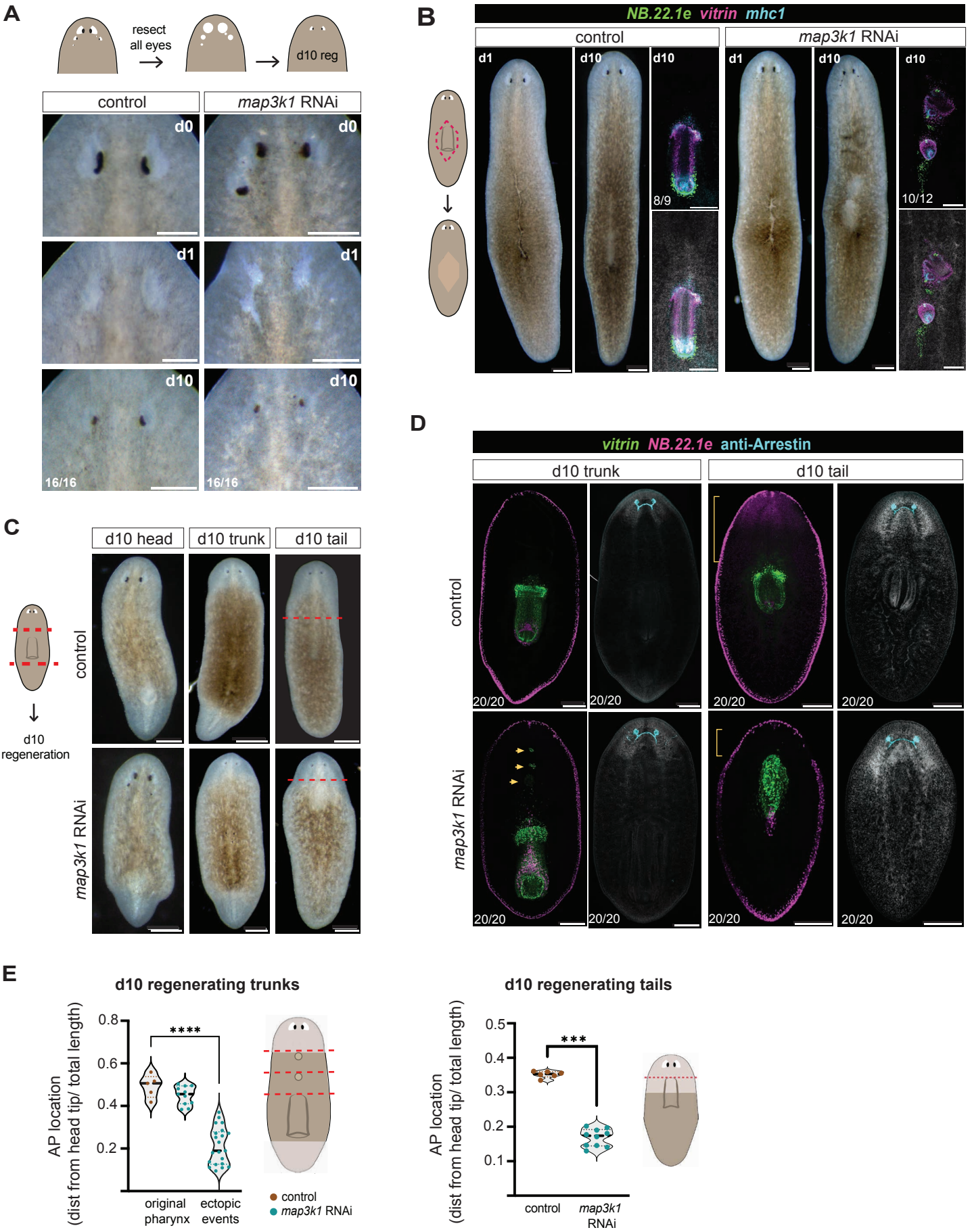
A
resect
all eyes
d10 reg
control
map3k1 RNAi
d0
d1
d10
16/16
B
NB.22.1e vitrin mhc1
control
map3k1 RNAi
d1
d10
8/9
10/12
C
d10 head
d10 trunk
d10 tail
control
map3k1 RNAi
d10
regeneration
D
vitrin NB.22.1e anti-Arrestin
d10 trunk
d10 tail
control
map3k1 RNAi
20/20
E
d10 regenerating trunks
AP location
(dist from head tip/ total length)
0.8
0.6
0.4
0.2
****
original
pharynx
ectopic
events
control
map3k1 RNAi
d10 regenerating tails
0.5
0.4
0.3
0.2
0.1
***
control
map3k1
RNAi

Figure 5

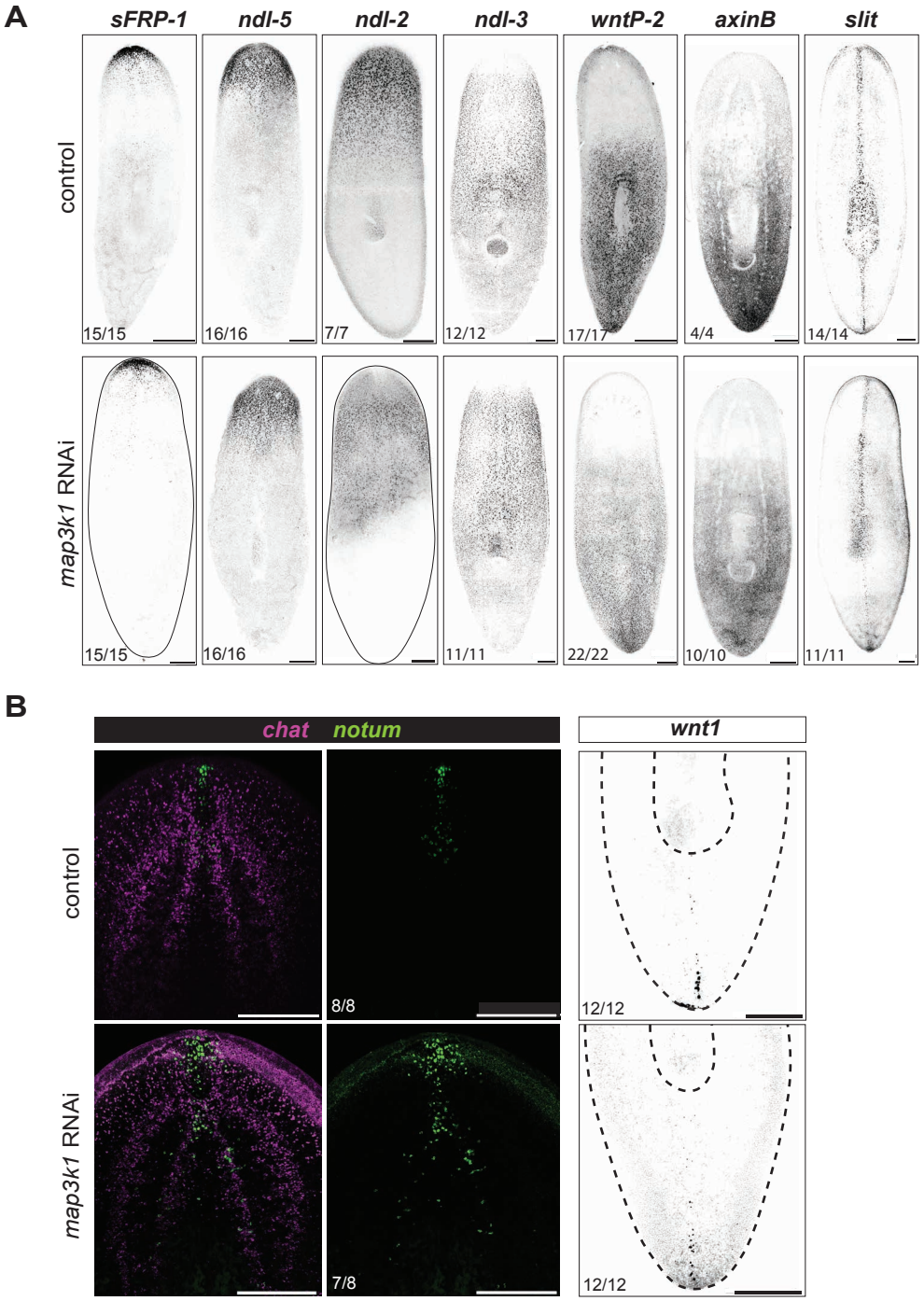
A
sFRP-1
ndl-5
ndl-2
ndl-3
wntP-2
axinB
slit
control
map3k1 RNAi
15/15
16/16
7/7
12/12
17/17
4/4
14/14
15/15
16/16
11/11
22/22
10/10
11/11
B
chat
notum
wnt1
control
map3k1 RNAi
8/8
12/12
7/8
12/12

Figure 6

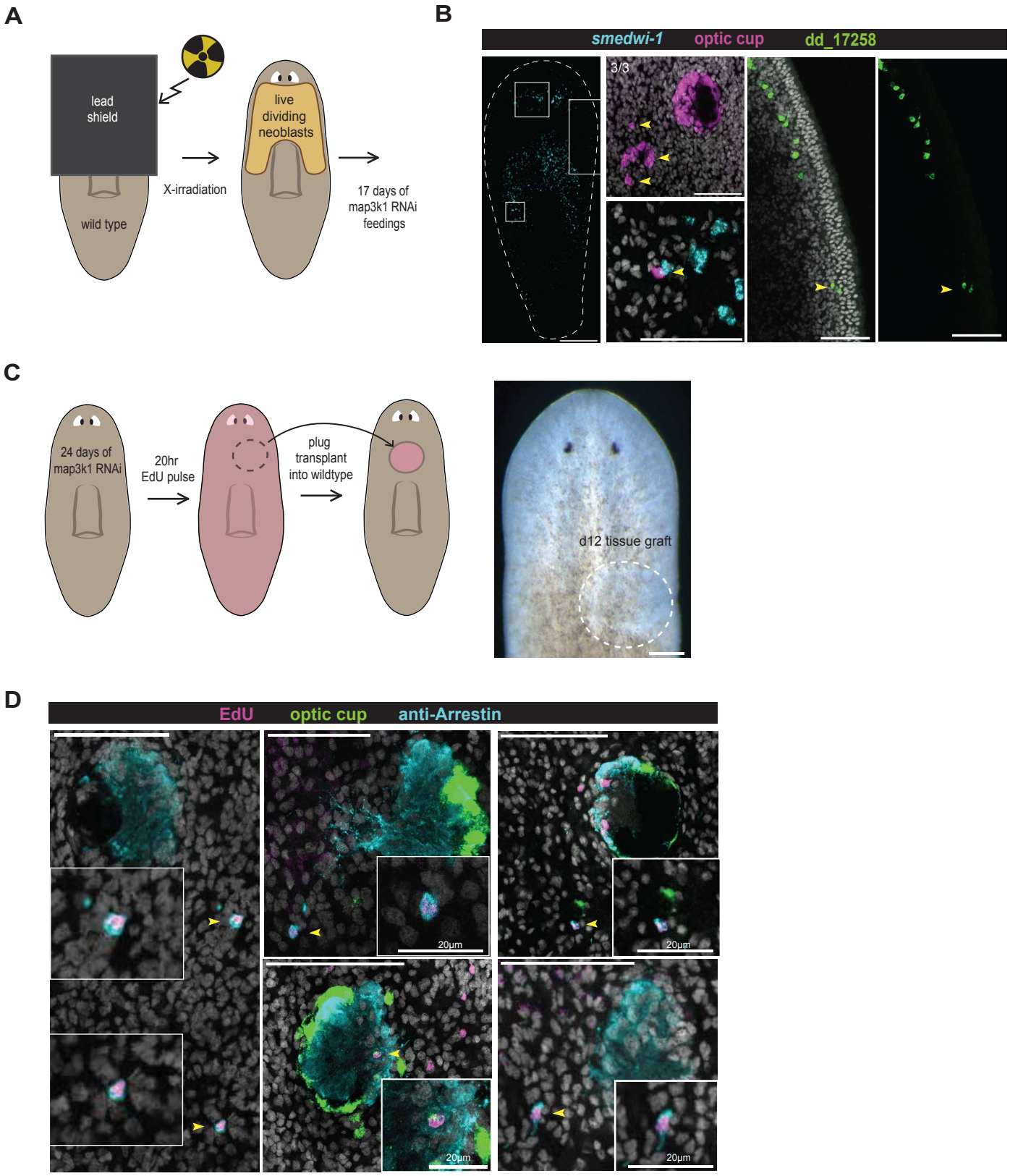
A
lead shield
wild type
X-irradiation
live dividing neoblasts
17 days of map3k1 RNAi feedings
B
smedwi-1
optic cup
dd_17258
3/3
C
24 days of map3k1 RNAi
20hr EdU pulse
plug transplant into wildtype
d12 tissue graft
D
EdU
optic cup
anti-Arrestin
20µm
20µm
20µm
20µm

Figure 7

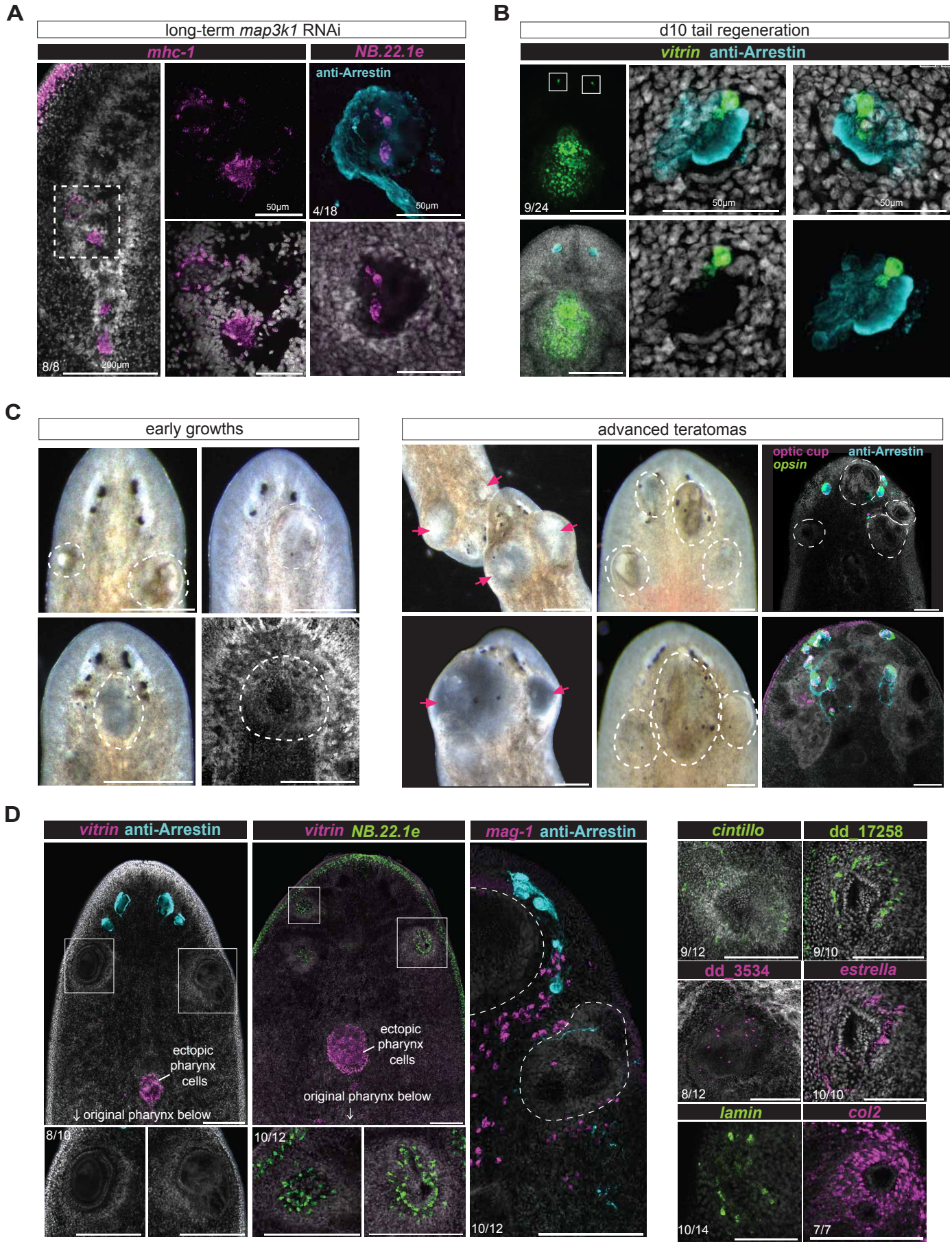
A
long-term map3k1 RNAi
mhc-1
NB.22.1e
anti-Arrestin
8/8
200µm
50µm
4/18
B
d10 tail regeneration
vitrin anti-Arrestin
9/24
50µm
C
early growths
advanced teratomas
optic cup
opsin
anti-Arrestin
D
vitrin anti-Arrestin
vitrin NB.22.1e
mag-1 anti-Arrestin
ectopic pharynx cells
original pharynx below
8/10
10/12
cintillo
dd_17258
9/12
9/10
dd_3534
estrella
8/12
10/10
lamin
col2
10/14
7/7

Figure 8

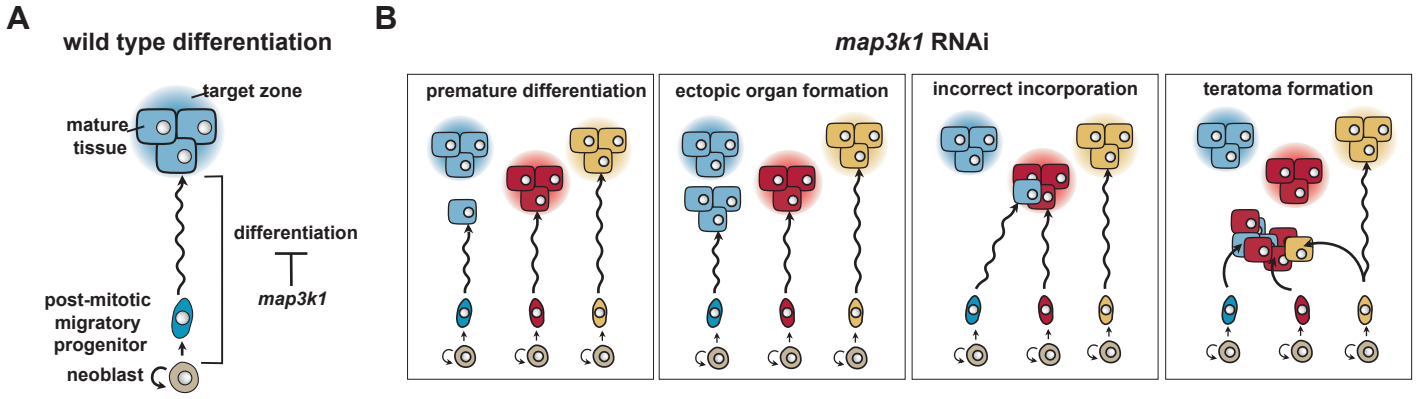
A
wild type differentiation
target zone
mature tissue
differentiation
map3k1
post-mitotic migratory progenitor
neoblast
B
map3k1 RNAi
premature differentiation
ectopic organ formation
incorrect incorporation
teratoma formation

Figure 1- figure supplement 1

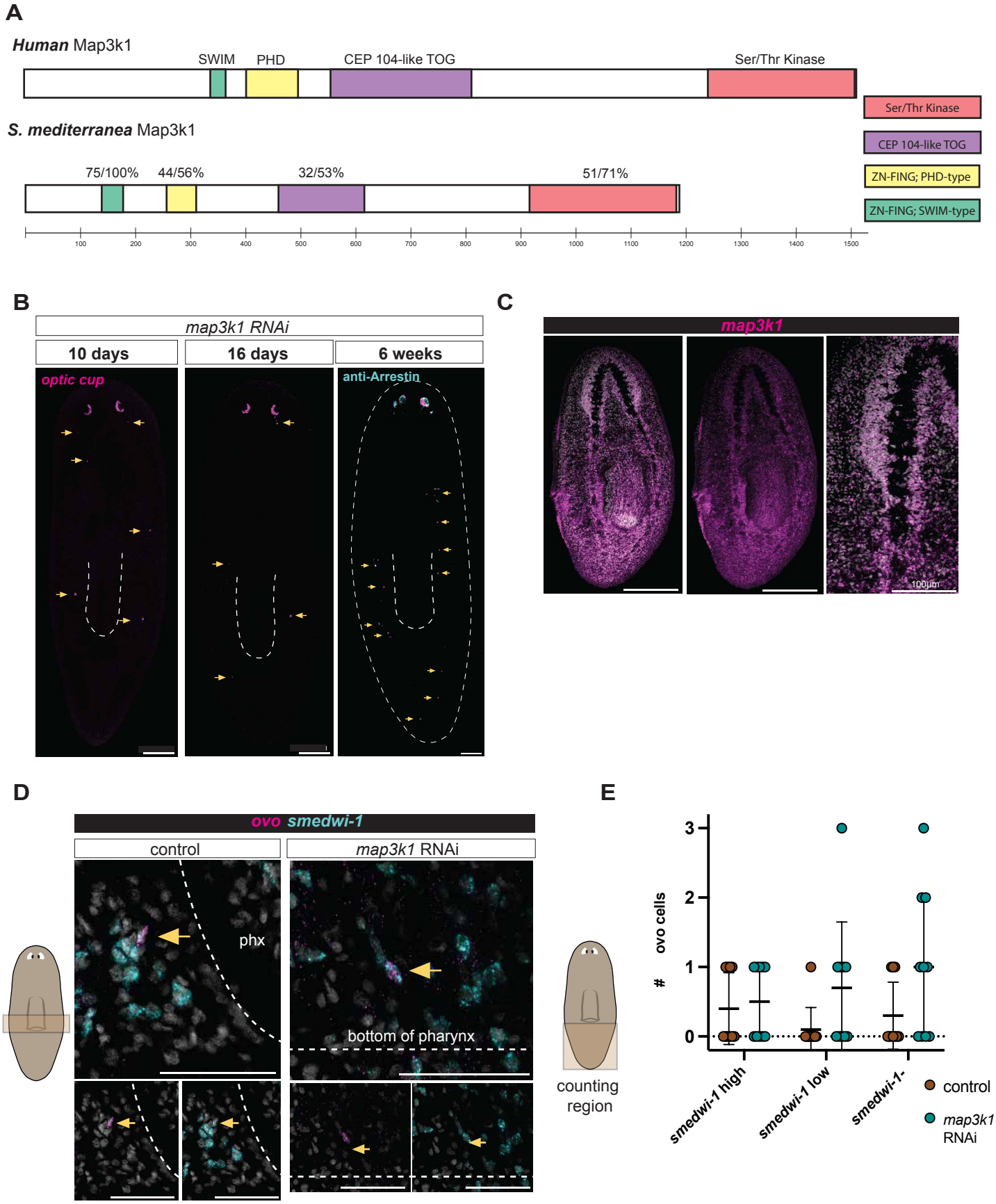

Figure 1- figure supplement 1. *map3k1* RNAi results in differentiated eye cells throughout the AP axis, and no overt change in eye progenitor distribution. A. Domain structure of human and *Schmidtea mediterranea* MAP3K1. % identity/ similarity is displayed above each domain. **B.** FISH of *map3k1* RNAi animals at 10 days, 16 days, and 6 weeks of RNAi shows optic cup (*catalase1, tyrosinase, glut3*) in the posterior at early timepoints. **C.** FISH with an RNA probe to the *map3k1* gene in a wild-type animal. Scale bar, 200μm for full body images; Scale bar, 100μm for closeup of the brain. **D.** FISH showing double-positive *ovo*+ ; *smedwi-1*+ cells near the posterior half of the pharynx. Scale bars, 50μm. **E.** quantification of *smedwi-1* high, *smedwi-1* low, and *smedwi-1* negative *ovo*+ cells in the tails of *map3k1* RNAi and control animals. No significant change is observed between the number of *smedwi-1*+ ; *ovo*+ cells in the tail between *map3k1* RNAi and control animals.

Figure 2- figure supplement 1

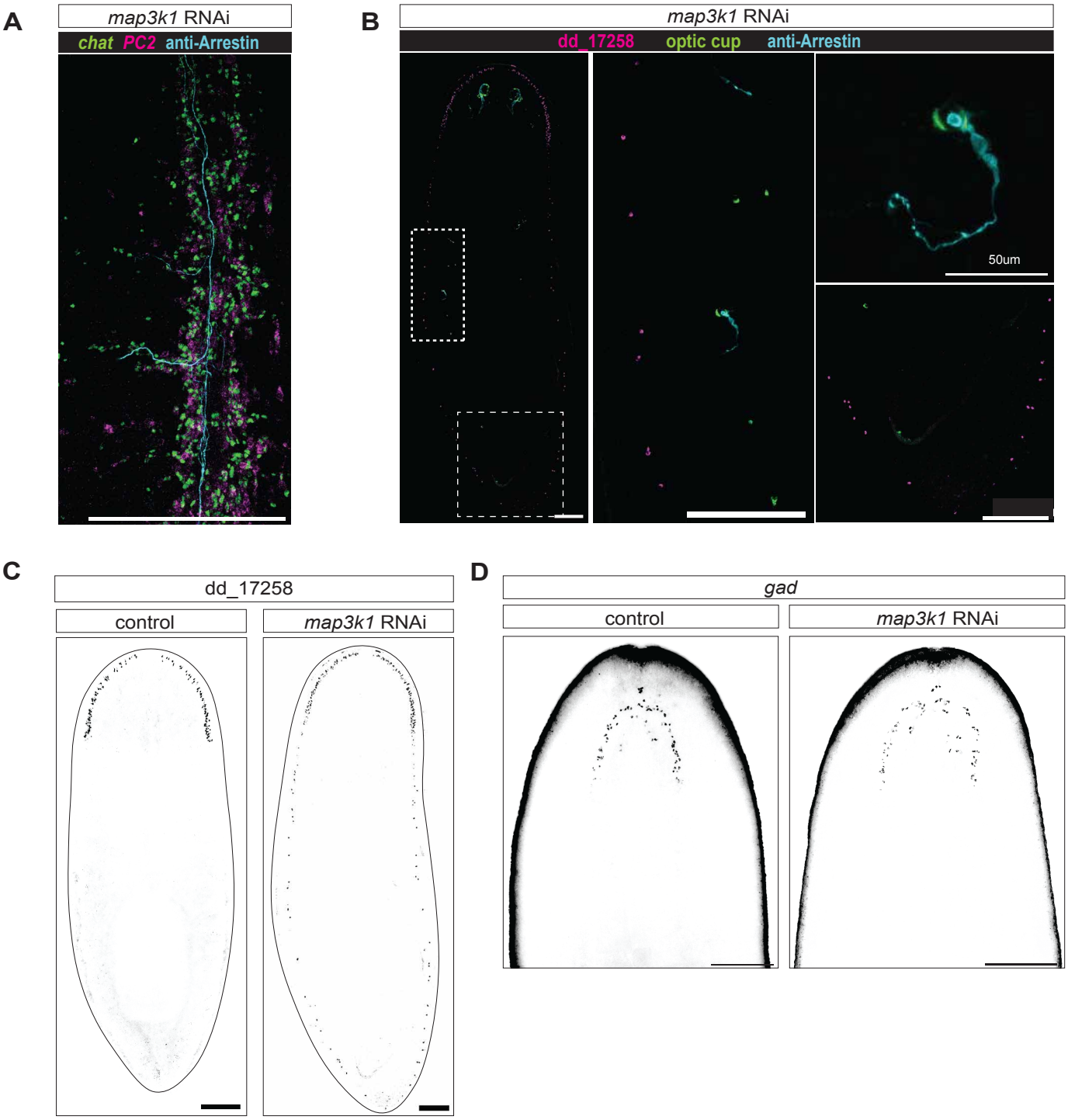

Figure 2- figure supplement 1. *map3k1* RNAi results ectopic brain branches posterior to the brain and posterior expansion of some neural cell types. A. Close-up FISH of ventral nerve cord (VNC) and branches in a *map3k1* RNAi animal. Photoreceptor projections (anti-Arrestin) are travel along the VNC and into ectopic branches labeled by the pan-neural markers *chat* and *pc2*. Scale bar, 100μm. **B.** FISH of dd_17258+ cells and optic cup cells (*catalase1, tyrosinase, glut3*), together with antibody labeling of photoreceptors (anti-Arrestin), extending down the AP axis. All scale bars, 200μm, unless otherwise specified in the lower left. **C.** FISH showing expansion of dd_17258 cells down the entire AP axis in a *map3k1* RNAi animal. Scale bar, 200μm. **D.** FISH showing an unchanged neural cell type (*gad*) in *map3k1* RNAi and control animals. Scale bar, 200μm.

Figure 4- figure supplement 1

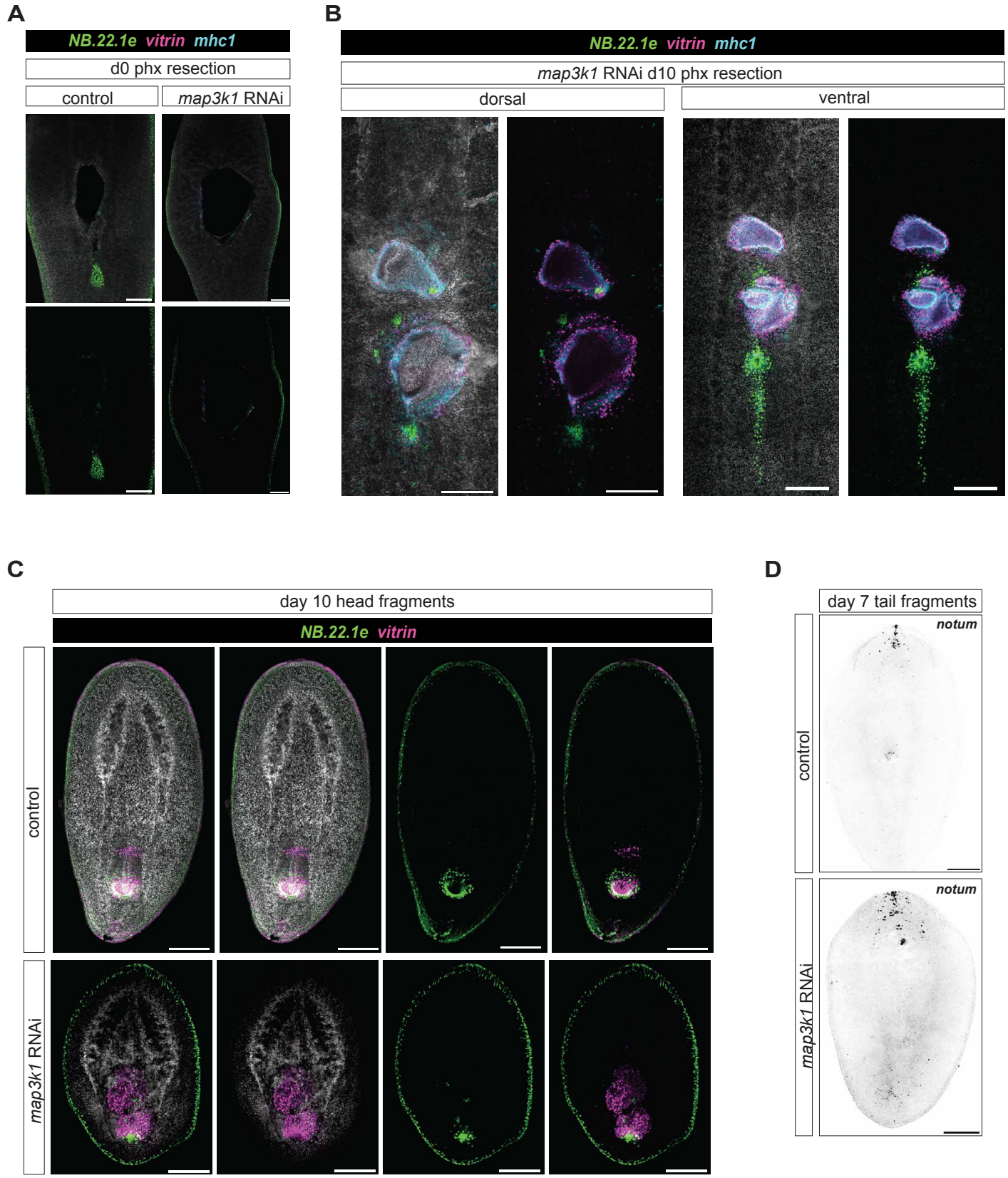

Figure 4- figure supplement 1. *map3k1* RNAi animals can undergo tissue-specific and whole-body regeneration, with some errors in pharynx organization. A. FISH following pharynx resection at day zero (d0) with the markers *vitrin* (pharynx-specific), *NB.22.1e* (mouth and esophagus), and *mhc1* (pharynx muscle). Scale bars, 200µm. **B.** Example of *map3k1* RNAi d10 pharynx resection. FISH shows dorsal (left) and ventral (right) views of the same animal, showing disorganized pharynx regeneration in *map3k1* RNAi animals. **C.** FISH of d10 head regeneration showing disorganized regeneration of the pharynx using *vitrin* and *NB.22.1e* RNA probes. Scale bars, 200µm. n=10/10. **D.** FISH showing dispersed *notum*+ cells in a d7 tail regenerate compared to control animals. Scale bar, 200µm

Figure 5- figure supplement 1

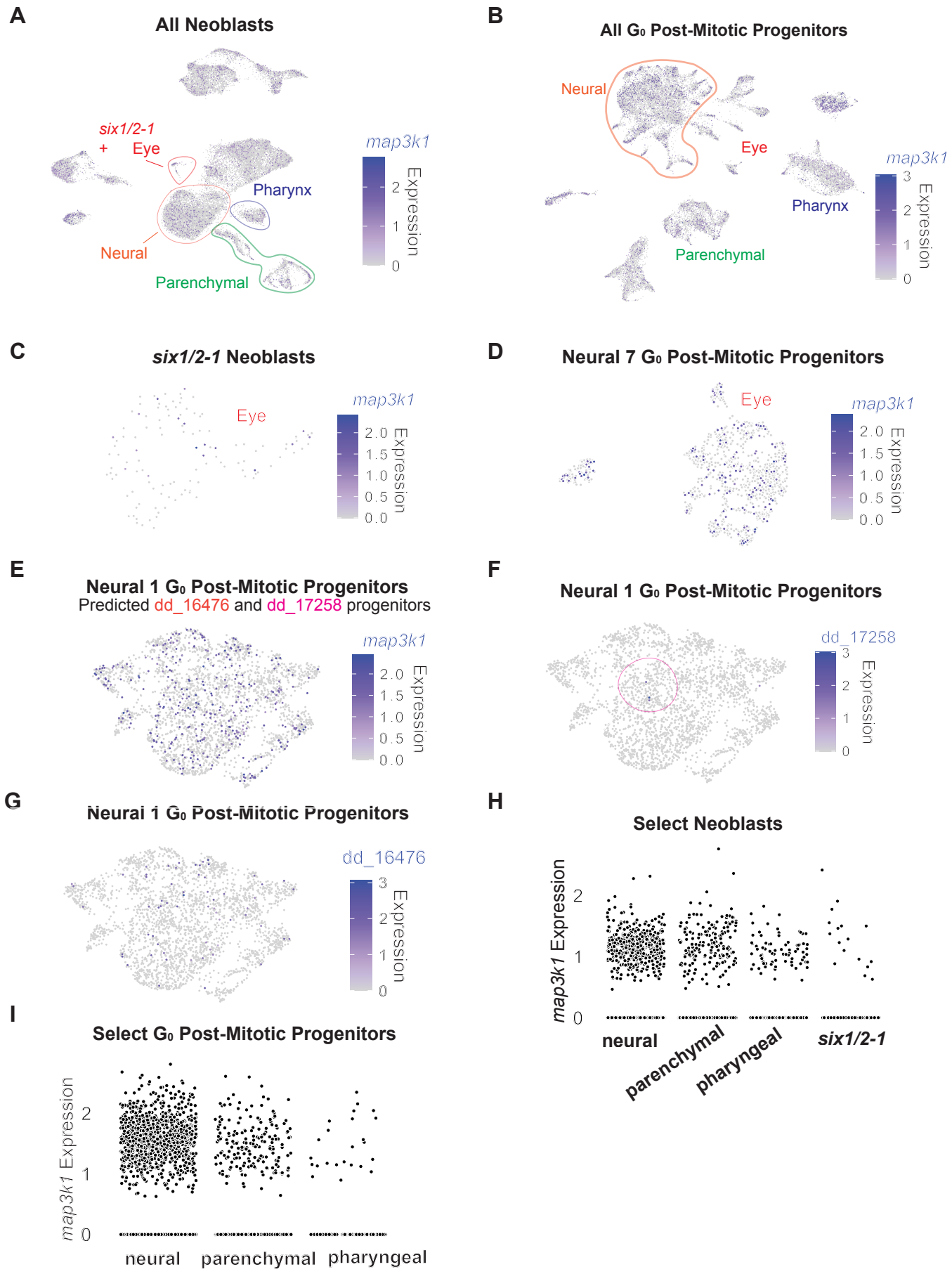

Figure 5- figure supplement 1. *map3k1 i*s expressed in neoblasts and post-mitotic progenitors. A. *map3k1* is expressed broadly across neoblast clusters. Plot points are ordered. **B.** *map3k1* is expressed broadly across post-mitotic progenitors; plot points are ordered. **C.** *map3k1* is expressed in some *six-1/2*+ neoblasts, which contain eye neoblasts; plot points are ordered. **D.** *map3k1* is expressed in some G0 post-mitotic eye progenitors; plot points are ordered. **E.** *map3k1* is expressed within the predicted progenitor cluster (Neural 1) of the affected cell types: dd_17258 and dd_16476; plot points are ordered. **F.** dd_17258 mature marker expression within its predicted progenitor cluster (Neural 1); plot points are ordered. **G.** dd_16476 mature marker expression within its predicted progenitor cluster (Neural 1); plot points are ordered. **H.** *map3k1* expression in neural, parenchymal, pharyngeal, and *six1/2*+ neoblast clusters. **I.** *map3k1* expression in neural, parenchymal, and pharyngeal post-mitotic progenitor clusters.

Figure 6 - figure supplement 1

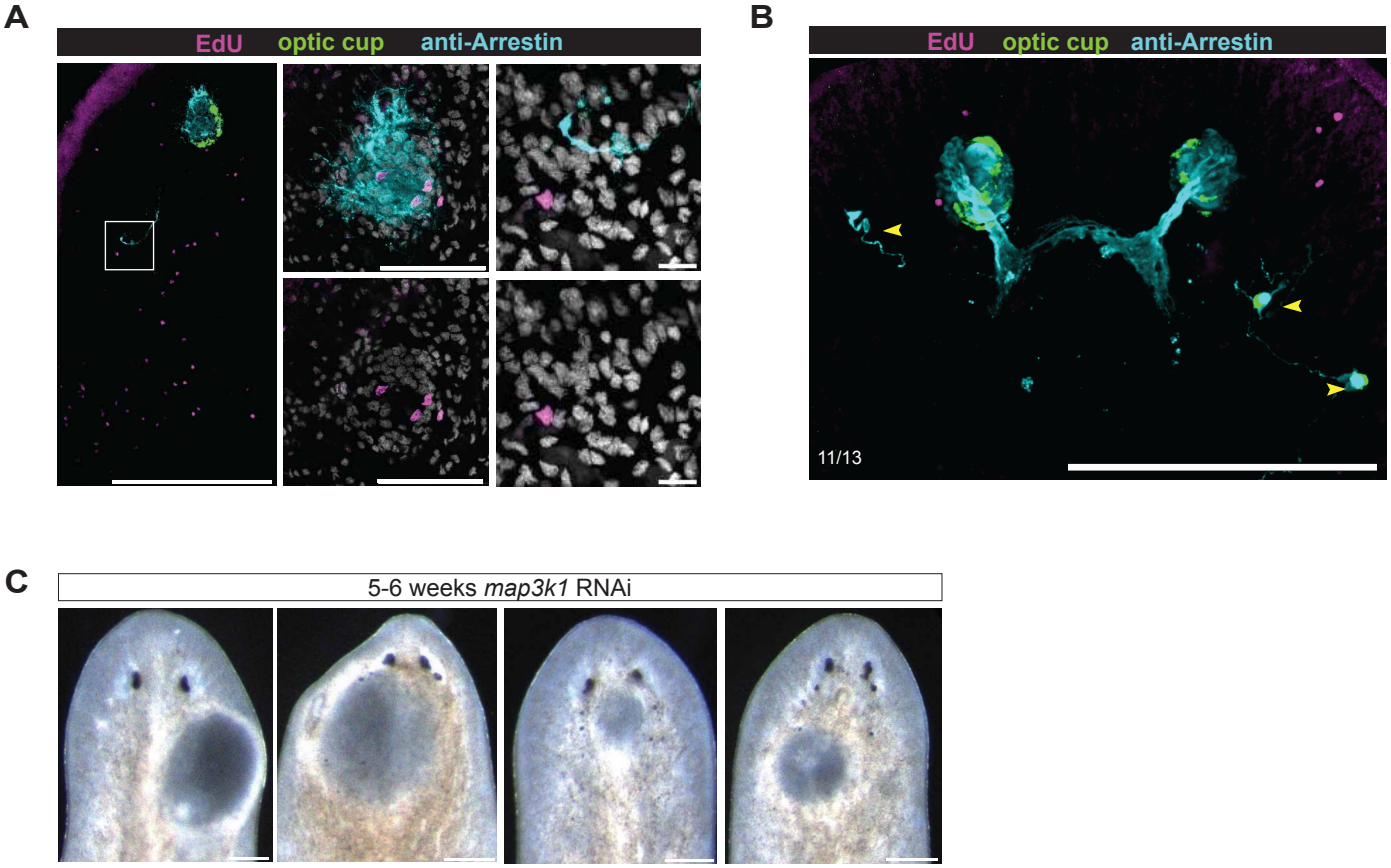

Figure 6- figure supplement 1. *map3k1* RNAi animals display to improper progenitor targeting and teratoma formation. **A.** FISH showing EdU+ photoreceptors (anti-Arrestin) in the eye of the recipient animal. These cells differentiated from *map3k1* RNAi progenitors born during the EdU pulse of the donor animal, following wild-type migratory cues out of the graft and into the recipient eye. Scale bar, 200μm. **B.** FISH image of EdU- ectopic eye cells in recipient wild-type animals after EdU plug transplantation. Scale bar, 200μm. **C.** Live images of early growths that will eventually become teratomas in *map3k1* RNAi animals. Scale bar, 100μm.